

Challenges and advances in the application of dynamic nuclear polarization to liquid-state samples

Nandita Abhyankar^{1,2}, Veronika Szalai^{2*}*

¹Institute for Research in Electronics and Applied Physics, University of Maryland, College Park, MD 20742, USA

²National Institute of Standards and Technology, Gaithersburg, MD 20899, USA

*Corresponding authors: nandita.abhyankar@nist.gov, vszalai@nist.gov

Abstract:

Nuclear magnetic resonance (NMR) spectroscopy is a powerful method to study structure and dynamics of materials. The inherently low sensitivity of NMR spectroscopy is a consequence of low spin polarization. Hyperpolarization of a spin ensemble is defined as a population difference between spin states that far exceeds what is expected from the Boltzmann distribution for a given temperature. Dynamic nuclear polarization (DNP) can overcome the relatively low sensitivity of NMR spectroscopy by using a paramagnetic matrix to hyperpolarize a nuclear spin ensemble. Application of DNP NMR can result in sensitivity gains of up to four orders of magnitude compared to NMR without DNP. Although DNP NMR is now more routinely available for solid-state NMR spectroscopy, it has not been exploited to the same degree for liquid-state samples. This review will consider challenges and advances in the application of DNP NMR to liquid-state samples. The review is organized into four sections: (i) mechanisms of DNP NMR relevant to hyperpolarization of liquid samples; (ii) applications of liquid-state DNP NMR; (iii) available detection schemes for liquid-state samples; and (iv) instrumental challenges and outlook for liquid-state DNP NMR.

27 **Introduction:**

28 Nuclear magnetic resonance transitions have small energy scales ($\Delta E \ll kT$; where ΔE is the
29 energy difference between magnetic energy levels, k is the Boltzmann constant, and T is
30 temperature of the system). Due to unfavorable Boltzmann factors ($N_{I=+1/2}/N_{I=-1/2} \approx 0.999999$ for
31 an ensemble of proton nuclear spins at 1 K and 1 T), nuclear spin ensembles have very low spin
32 polarization. The resulting low sensitivity of this method hinders its application to samples with
33 limited mass, volume, or concentration. Development of instrumentation for high-field and low-
34 temperature NMR has greatly improved detection limits but nuclear spin polarization is low even
35 under these demanding conditions. Apart from these so-called ‘brute force’ strategies to increase
36 spin polarization, dynamic nuclear polarization (DNP) has gained significant attention in the past
37 few decades. In DNP, polarization is transferred from an electron spin ensemble to a nuclear spin
38 ensemble; the large difference in timescales of relaxation of electron spins and nuclear spins results
39 in hyperpolarization of the nuclear spin ensemble. Compared to nuclear spin ensembles, electron
40 spin ensembles have much higher polarization as a result of the thousand-fold or greater advantage
41 provided by the higher gyromagnetic ratio of an electron compared to nuclei. Secondly, the
42 relaxation processes of an electron spin ensemble are much faster than those of a nuclear spin
43 ensemble. DNP exploits these disparities to transfer polarization from electrons to nuclei, resulting
44 in hyperpolarization of the nuclear spin ensemble. Most notably, the combination of DNP with
45 magic angle spinning (MAS) has resulted in phenomenal improvements in sensitivity for solid-
46 state samples.¹ In contrast, DNP NMR in the liquid state has not been explored to the same extent,
47 despite its potential utility in applications such as nuclear magnetic resonance imaging and high-
48 resolution NMR spectroscopy of biological samples.

49 Solid-state magnetic resonance spectra are broadened by dipolar interactions, anisotropies of
50 chemical shift, and in some cases, anisotropies of quadrupolar interactions. Motional averaging
51 removes this broadening in liquid-state experiments, yielding high-resolution spectra that contain
52 information about structure and dynamics of molecules in solution. Liquid DNP NMR has the
53 potential to provide information that is presently inaccessible, particularly regarding dynamic
54 processes that only occur under physiological conditions or in the liquid state. Such processes
55 include reaction mechanisms, kinetics, and evolving chemical profiles of complex mixtures.
56 Imaging of tissues necessarily involves aqueous solutions and is typically performed at ambient
57 temperature. Spectroscopy at physiological temperatures is also important for determination of
58 structure-function relationships in biomacromolecules. The sensitivity gains obtained from DNP
59 make it particularly applicable to the study of low-concentration, mass-limited samples, such as
60 transient species in reactions and aggregation-prone biomacromolecules. Membrane proteins, for
61 example, are extremely challenging to study because their concentration must be limited due to
62 their tendency to aggregate. Recent progress in DNP NMR with magic angle spinning (MAS) has
63 been highly impactful in protein structure studies by improving sensitivity as well as resolution.
64 Lyophilized membrane proteins allow solid-state (ss) NMR to be conducted at ambient
65 temperatures. However, the protocols for sample preparation for ss NMR are not well-defined.²
66 Liquid DNP NMR is a more general approach suitable for a broad range of samples. It can provide
67 information about dynamic processes such as conformational changes, protein-ligand interactions,
68 and changes in solvation during structural transformations. Liquid DNP NMR has the most
69 potential for impact in spatio-temporal studies which must necessarily be conducted in the liquid
70 state and are hindered by the small concentrations of transient species -- e.g., studies of solvation
71 dynamics, reaction kinetics, metabolite profiling, and imaging. Such studies would benefit greatly

72 from the sensitivity gains provided by DNP NMR. Section II provides examples of the benefits of
73 liquid DNP NMR for these fields.

74 Several comprehensive reviews of DNP NMR, especially under the high-field conditions of
75 modern NMR, are available.^{1,3,4,5} There are also more recent reviews of liquid-state NMR.^{6,7,8}
76 These reviews provide an understanding of the mechanistic aspects of DNP NMR and particular
77 methodological developments. In this review, we aim to highlight how hyperpolarization through
78 DNP can be employed to achieve sensitivity gains for liquid-state NMR spectroscopy. We will
79 consider the current scope, applications, opportunities for development, and experimental
80 challenges hindering widespread adoption of liquid-state DNP NMR spectroscopy as an analytical
81 tool. In Section I, we provide a brief description of the mechanisms of liquid DNP NMR, including
82 both solid-state and liquid-state mechanisms because both are applied for liquid DNP NMR. In
83 section II, we discuss potential applications that are particularly suitable for liquid DNP NMR. In
84 Section III, we review available detection schemes that exploit various mechanisms. Finally, in
85 Section IV, we attempt to delineate the challenges associated with these detection schemes, and
86 survey future research directions in the development of instrumentation for DNP NMR for liquid-
87 state samples.

88 **Section I: Mechanisms relevant to liquid DNP NMR.**

89 We shall consider only mechanisms for steady-state or continuous-wave (CW) DNP of insulators
90 since these are predominantly applied in present-day DNP NMR detection schemes. In CW DNP,
91 microwaves are continuously applied to the sample containing the paramagnetic material, called
92 the polarizing agent (PA), in order to saturate the electron paramagnetic resonance (EPR)
93 transition. Under optimal conditions defined by microwave frequency, magnetic field, and
94 temperature, hyperpolarization of the nuclear spin ensemble results from the dynamic process of

95 spin-lattice relaxation of the polarized electron spin ensemble, resulting in transfer of spin
 96 polarization from electrons to nuclei. Following this process, Fourier transform (FT) NMR is
 97 conducted on the hyperpolarized nuclear spin ensemble using pulse schema.

98 Of the CW mechanisms, only the Overhauser effect is directly applicable to solutions. Here we
 99 first provide a brief description of the Overhauser effect. We will also describe, albeit qualitatively,
 100 solid-state DNP mechanisms (solid effect, cross effect, and thermal mixing) since these can be
 101 exploited by conducting DNP in the frozen, solid state, followed by rapid melting/dissolution and
 102 detection of NMR in the liquid state. The reader is directed to papers that provide in-depth
 103 mathematical discussions of these mechanisms and their theoretical limits. Finally, we will briefly
 104 discuss why integrating DNP with high-field NMR is challenging.

105 Electron-nuclear coupling through the hyperfine interaction (HFI) is the basis of all DNP
 106 mechanisms. In the first step of CW DNP, an electron spin ensemble in a static magnetic field is
 107 irradiated with high-intensity microwaves to saturate its electron spin resonance (see Figure 2a),
 108 creating a non-equilibrium state. Coupling between an electron and nucleus is mediated by the
 109 hyperfine interaction (HFI), which can be composed of the isotropic (scalar) Fermi contact term
 110 and/or the anisotropic dipolar term. The spin Hamiltonian \hat{H} for a coupled two-spin (electron –
 111 nucleus, $S = 1/2$, $I = 1/2$) system is shown in the high-field limit, where the static field is applied in
 112 the z direction and all other terms can be treated as perturbations to the electron Zeeman term H_S :

$$113 \quad \hat{H} = \hat{H}_S + \hat{H}_I + \hat{H}_{SI} = \omega_{0S}\hat{S}_z - \omega_{0I}\hat{I}_z + \hat{A}_{SI}^{FC} + \hat{A}_{SI}^{dip}(\mathbf{Eq. 1});$$

114 where \hat{H}_S is electron Zeeman term, \hat{H}_I is the nuclear Zeeman term, \hat{H}_{SI} is the hyperfine term, ω_{0S}
 115 and ω_{0I} are the electron and nuclear Larmor frequencies respectively, \hat{S}_z and \hat{I}_z are the z -
 116 components of the electron and nuclear spin operators respectively, \hat{A}_{SI}^{FC} is the Fermi contact

117 (scalar) part of the HFI (see Eq. 2 below) and \hat{A}_{SI}^{dip} is the distance-dependent, anisotropic dipolar
 118 part of the HFI (see Eq. 3 below).

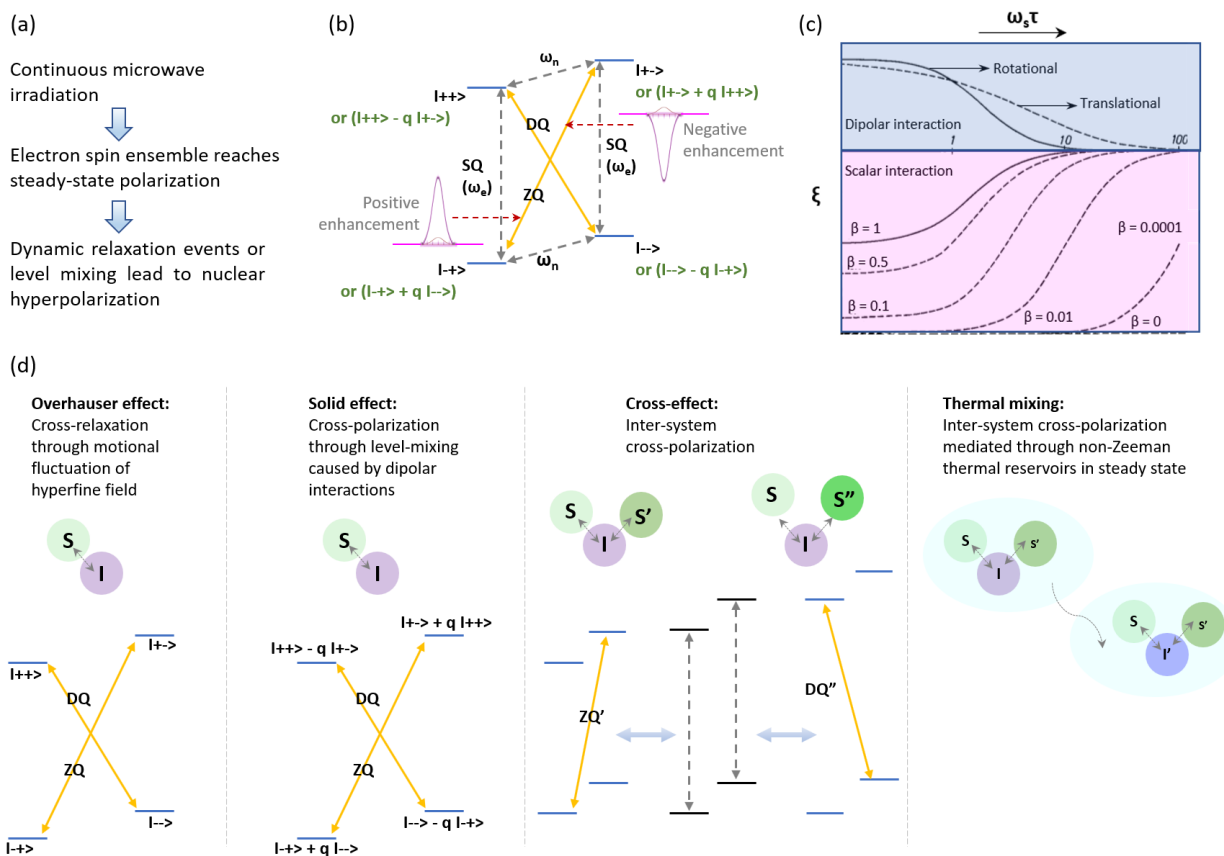
119
$$\hat{A}_{SI}^{FC} = \frac{\gamma_S \gamma_I \hbar^2 8\pi}{3} |\psi(0)|^2 \mathbf{I} \cdot \mathbf{S} \text{ (Eq. 2);}$$

120 where γ_S and γ_I are the gyromagnetic ratios of the electron and proton respectively, and $\psi(0)$ is
 121 the electron spin density at the nucleus (s-electron density is the only contributor to this term).

122
$$\hat{A}_{SI}^{dip} = \gamma_S \gamma_I \hbar^2 \left[\frac{\mathbf{I} \cdot \mathbf{S}}{r^3} \right] - \frac{3(\mathbf{I} \cdot \mathbf{r})(\mathbf{S} \cdot \mathbf{r})}{r^5} \text{ (Eq. 3);}$$

123 Figure 2b shows the eigen level diagram and possible transitions in the coupled two-spin (electron-
 124 proton; $S = 1/2$, $I = 1/2$) system described above. Single-quantum (SQ) transitions are the allowed
 125 transitions in conventional perpendicular-mode EPR excitation (excitation field B_1 applied
 126 perpendicular to static field B_0). They are described by the selection rule $\Delta m_S = \pm 1$, $\Delta m_I = 0$.
 127 Double quantum (DQ) and zero quantum (ZQ) transitions involve simultaneous electron and
 128 nuclear spin flips and are forbidden. However, it is precisely these forbidden transitions that
 129 provide the cross-polarization pathways resulting in nuclear hyperpolarization. Selective driving
 130 of either the ZQ or DQ transition results in ‘overpopulation’ of the $|-\rangle$ or $|+\rangle$ nuclear state,
 131 respectively, resulting in a population difference much higher than that expected from the
 132 Boltzmann thermal distribution. Hyperpolarization through the ZQ transition overpopulates the
 133 lower nuclear energy level, resulting in positive enhancement of the NMR signal. Conversely,
 134 hyperpolarization through the DQ transition results in negative enhancement of the NMR signal.

135



137

138 **Figure 1:** Common features of continuous-wave dynamic nuclear polarization mechanisms. (a)
 139 Schematic of steps to produce a hyperpolarized nuclear ensemble using DNP under steady-state
 140 microwave irradiation. (b) Cartoon representation of eigen levels of an electron-nucleus (two-spin)
 141 system with $S = \frac{1}{2}$ and $I = \frac{1}{2}$. ω_e and ω_N are the allowed single quantum transitions (Δm_S (Δm_I) =
 142 ± 1 , Δm_I (Δm_S) = 0) It should be noted that the differences between electronic energy levels are at
 143 least three orders of magnitude larger than differences between nuclear energy levels, i.e. $\omega_e \gg \gg \omega_N$. Dipolar and/or scalar components of the hyperfine interaction can facilitate the forbidden
 144 double quantum (DQ) and zero quantum (ZQ) transitions. Selectively driving either the DQ or ZQ
 145 transition leads to nuclear hyperpolarization. (c) Frequency/field-dependence of ODNP
 146 enhancement coupling factor (ξ) for modulation of dipolar and scalar components of HFI.
 147 (Adapted with permission from ref. 9 Copyright 1968 Elsevier) See text below for an explanation
 148 of the factor β . (d) Schematic of cross-polarization processes that lead to hyperpolarization in the
 149 four broad classes of mechanisms.

151

152

153 It is evident from the above explanation that the success of DNP depends on two factors: first,
154 increasing the probability of the forbidden ZQ or DQ transition and second, the ability to
155 selectively drive either the ZQ or the DQ transition. The HFI can mediate these nominally
156 forbidden transitions in two ways:

157 i. Random fluctuations in the hyperfine term can provide a cross-relaxation pathway to
158 transfer polarization from the electron spin ensemble to the nuclear spin ensemble. This
159 is the mechanism of DNP proposed originally by Overhauser for metals. In metals,
160 electron delocalization causes random fluctuations of the electronic wave function,
161 which results in cross-relaxation from the electron spin ensemble to the nuclear spin
162 ensemble through the scalar part of the HFI.¹⁰ In insulating liquids, these random
163 fluctuations are provided by translational or rotational diffusion of molecules.¹¹ DNP
164 enhancement of the NMR signal is maximized when the rate of fluctuation of the
165 hyperfine term matches the frequency associated with the ZQ or DQ transition.

166 ii. The dipolar part of the HFI can result in mixing of nuclear states, allowing direct
167 excitation of the nominally forbidden ZQ and DQ transitions. This is the basis of the
168 ‘solid effect’, which describes DNP enhancement in insulating solids.¹¹

169 Dipolar coupling can induce SQ, ZQ, and DQ transitions while scalar coupling induces ZQ
170 transitions selectively.

171 Whereas the Overhauser effect and solid effect are two-spin mechanisms, the cross-effect and
172 thermal mixing are three-spin mechanisms that may be thought of simplistically as cross-
173 polarization through coupling of two different electron-nucleus systems sharing the same nucleus.
174 Often, a combination of mechanisms is observed, with one being dominant depending on the
175 choice of physical conditions, PA, and concentration of PA. The study of nuclear hyperpolarization

176 mechanisms is an active field, with ongoing theoretical and experimental work to elucidate and
177 quantify various factors that determine DNP enhancement. Below, we describe characteristics of
178 the four main classes of DNP mechanisms relevant to liquid DNP NMR. We delineate the
179 interactions responsible for transfer of polarization from electrons to nuclei, conditions for
180 observing DNP, and how DNP enhancement is affected by field strength for each mechanism. The
181 Overhauser effect is described in greater detail while the solid effect, cross effect, and thermal
182 mixing are described qualitatively. Theoretical work on solid-state mechanisms is ongoing and the
183 interested reader is directed to papers describing these effects in greater detail.

184
185 1. **Overhauser effect:** This is the only mechanism that can result in direct DNP enhancement in
186 the liquid state. Overhauser predicted that the spin polarization of a bath of conduction-
187 electrons could be transferred to a nuclear spin ensemble. Spin polarization of the conduction-
188 electron spin ensemble must first be saturated by irradiation with microwaves of frequency ω_0 .
189 Cross-relaxation through the Fermi contact term of the HFI (H_{SI} , *Eq. 1*) results in
190 hyperpolarization.¹⁰ This effect, which he thought would only apply to the case of metals, was
191 verified experimentally by Carver and Slichter for metallic lithium.¹² Abragam pointed out the
192 mechanisms by which Overhauser enhancement could be achieved for insulating solids and
193 solutions.^{11,13} In Overhauser DNP of paramagnetic ions in solution, electron-nuclear (e-n)
194 cross-relaxation can occur through stochastic fluctuations of the dipolar and/or scalar parts of
195 the HFI. Time-dependence of the dipolar part of the HFI in solutions may be associated with
196 electron spin relaxation, electron spin exchange, chemical exchange, or translational/rotational
197 motions. On the other hand, time-dependence of scalar interactions is typically associated with
198 processes that change the electronic configuration and s-electron density of the paramagnetic
199 species, including electron spin relaxation, electron spin exchange, and chemical exchange.⁹

200 Under the condition that electron spins relax much faster than nuclear spins, Solomon
 201 described the enhancement in steady-state nuclear spin polarization as:¹⁴

$$202 \quad \frac{\langle I_z \rangle}{I_0} = 1 + \left(\frac{w_2 - w_0}{w_0 + 2w_I + w_2} \right) \left(\frac{w_0 + 2w_1 + w_2}{w_0 + 2w_1 + w_2 + w^0} \right) \left(\frac{\langle S_0 \rangle - \langle S_z \rangle}{\langle S_0 \rangle} \right) \quad (\mathbf{Eq. 4});$$

203 Here, w_0 and w_2 represent the transition rates for the ZQ and DQ transitions respectively. w_I
 204 represents the rate of the single quantum nuclear transition ($\Delta I = \pm 1$, $\Delta S = 0$) while w_0
 205 represents the rate of nuclear spin relaxation through all other means besides electron-nuclear
 206 coupling.

207 *Eq. 4* may be rewritten as *Eq. 5* to define the factors that determine DNP enhancement via the
 208 Overhauser effect.

$$209 \quad \varepsilon = 1 - \xi f s \frac{\gamma_S}{\gamma_I} \quad (\mathbf{Eq. 5}); \text{ where}$$

$$210 \quad \xi = \frac{w_2 - w_0}{w_0 + 2w_N + w_2} \quad (\mathbf{Eq. 6}); \quad f = \frac{w_0 + 2w_1 + w_2}{w_0 + 2w_1 + w_2 + w^0} \quad (\mathbf{Eq. 7}); \quad s = \frac{\langle S_0 \rangle - \langle S_z \rangle}{\langle S_0 \rangle} \quad (\mathbf{Eq. 8})$$

211 The enhancement of nuclear spin polarization, $\mathcal{E} = \frac{\langle I_z \rangle}{I_0}$, is then a function of three factors: (i)
 212 the coupling factor, ξ , which is the ratio of polarization enhancement through selectivity of the
 213 DQ or ZQ transition over relaxation through all other competing transitions; (ii) the leakage
 214 factor, f , which describes how much of nuclear relaxation is caused by coupling to the electron
 215 spin (when $f = 1$, nuclear spin relaxation is exclusively through coupling to the electron spin
 216 and when $f = 0$, electron-nuclear coupling does not contribute to nuclear spin relaxation); and
 217 (iii) the saturation factor, s , which describes how completely the electron spin resonance
 218 transition can be saturated.

219 As mentioned earlier, enhancements from DQ transitions offset those from ZQ transitions.
 220 *Eq. 6* indicates that the enhancement factor increases as the rates of DQ and ZQ transitions
 221 become well separated so that one can be driven selectively over the other. DQ transitions
 222 result in positive enhancement of nuclear polarization while ZQ transitions result in negative
 223 enhancement. Enhancement factors on the order of 10^4 - 10^5 have been reported for liquid-state
 224 samples.¹⁵

225 **Decrease in ODNP enhancement at high fields.** The DNP enhancement depends on the
 226 coupling factor (*Eq. 6*), which in turn is a function of the transition rates for the DQ, ZQ, and
 227 nuclear single-quantum transitions. In liquids, HFI may be modulated by stochastic
 228 fluctuations of the dipolar HFI, scalar HFI, or a mixture of both. As mentioned above, time-
 229 dependence of the dipolar HFI may be associated with relaxation and exchange of the electron
 230 spin, chemical exchange, as well as rotational and translational diffusion. On the other hand,
 231 time-dependence of the scalar HFI can only be a result of electron spin relaxation, electron
 232 spin exchange or chemical exchange. The spectral density functions $j_d(\omega)$ and $j_s(\omega)$ describe
 233 the match between the ZQ/DQ transition frequencies and the modulation frequency of the HFI.
 234 The coupling factor for a system with a mixture of dipolar and scalar HFI can be described in
 235 terms of the spectral density functions:⁹

$$236 \quad \xi = \frac{M_d j_{d_2}(\omega_s) - M_s \frac{\tau_{s_2}}{\tau_{d_2}} j_{s_2}(\omega_s)}{M_d \left\{ \frac{7}{5} j_{d_2}(\omega_s) + \frac{3\tau_{d_1}}{5\tau_{d_2}} j_{d_1}(\omega_l) \right\} + M_s \left\{ \frac{\tau_{s_2}}{\tau_{d_2}} j_{s_2}(\omega_s) + \beta \frac{\tau_{s_1}}{\tau_{s_2}} j_{s_1}(\omega_l) \right\}} \quad (\text{Eq. 8})$$

237 Here, the subscripts *l* and *2* stand for longitudinal and transverse components as used in the
 238 Bloch formulation. M_d and M_s are the components of the mixing parameter M , which is the
 239 ratio of scalar to dipolar coupling. β describes the attenuation of the scalar enhancement due
 240 to spin exchange. It can range between 0 and 1, where $\beta = 0$ indicates no spin exchange.

241 The spectral density functions for time-dependence of the scalar and dipolar HFI are given by
242 the following equations:

$$243 \quad j_d(\omega) = \frac{1}{1 + \omega^2 \tau_d^2} \text{ (Eq .10)} \text{ and } j_s(\omega) = \frac{1}{1 + \omega^2 \tau_s^2} \text{ (Eq .11)}$$

244 where ω is the frequency of the ZQ/DQ transition and τ is the correlation time for the associated
245 HFI modulation. These equations indicate that when $\omega_s \gg 1/\tau$, the spectral density function
246 for cross-relaxation becomes vanishingly small, with a corresponding decrease in the coupling
247 factor. This describes the case at high fields, where the Zeeman splitting becomes much larger
248 than the modulation frequency of the HFI, e.g., when molecular motions are no longer fast
249 enough to facilitate the ZQ/DQ transitions. Similarly, in solids, the transverse fields provided
250 by the electron-nuclear dipolar interaction are too small to allow mixing of nuclear energy
251 levels at high fields. Therefore, DNP generally becomes less efficient at high fields.

252 Scalar enhancement occurs exclusively through the Fermi contact interaction. It is in principle
253 independent of field and can allow DNP to be conducted at high fields.^{6, 16} However, this
254 situation is rarely observed because DNP enhancement in samples with a scalar HFI
255 contribution is often attenuated by spin exchange processes ($\beta > 0$). Thus, the coupling factor
256 can range from -1 to +0.5, where $\xi = +0.5$ indicates purely dipolar modulation of HFI and $\xi =$
257 -1 indicates purely scalar modulation of HFI (Figure 1c).

258 2. **Solid effect:** Abragam described how DNP could occur in an insulating solid containing a
259 small concentration of paramagnetic impurities.¹¹ In this case, hyperpolarization of the nuclear
260 spin ensemble is achieved through direct excitation of DQ and ZQ transitions by microwave
261 irradiation of frequency $\omega_{0S} \pm \omega_{0I}$. Dipolar electron-nuclear interactions cause a slight tilting
262 of nuclear magnetic moments, resulting in energy level mixing that facilitates the nominally

263 forbidden DQ and ZQ transitions. The degree of mixing is described in terms of the factor q ,
264 which describes the dipolar coupling between the electron and nucleus:

$$265 \quad q = -\frac{3}{4} \frac{\gamma_S \gamma_I}{\omega_{0I}} \frac{1}{r^3} \sin\theta \cos\theta e^{-i\varphi} - \mathbf{Eq. 9}$$

266 Microwave frequency ($\omega_{0S} - \omega_{0I}$) drives the DQ transition while ($\omega_{0S} + \omega_{0I}$) drives the ZQ
267 transition (Table 1). As mentioned in the description of the Overhauser effect, driving the DQ
268 transition results in positive enhancement while the ZQ transition results in negative
269 enhancement. To ensure that these two enhancements do not cancel each other out, it is
270 desirable to selectively drive one of the two forbidden transitions by fulfilling the condition
271 that the EPR linewidth must be much smaller than ω_{0I} .

272 **Field dependence of SE:** As with the Overhauser effect, the solid effect also becomes less
273 efficient at higher fields. At low to intermediate fields, the spin temperature and dipolar
274 temperature become comparable.¹¹ The resulting quasi-continuous energy level distribution at
275 low fields increases the efficiency of cross-relaxation between spin levels. In contrast, at high
276 fields, spin temperature and dipolar temperature are well-separated in magnitude. Therefore,
277 the solid effect becomes less efficient as the field is increased. The solid effect may also be
278 observed in viscous liquids. For examples, the rotational correlation time of vanadyl complexes
279 is slow enough to result in DNP enhancement through the solid effect while yielding liquid-
280 state NMR spectra of protons, which have a much faster rotational correlation timescale.¹⁷

281 3. **Cross effect and thermal mixing:** Other than the two-spin mechanisms described above, there
282 are two other broad classes of mechanisms that are characterized by DNP enhancements that
283 increase with the concentration of the paramagnetic material. Hwang and Hill reported a new
284 hyperpolarization mechanism that is distinguishable from the solid effect because of the field
285 profile of the enhancement factor (Table 1).¹⁸ In this mechanism, the peaks in positive and

286 negative enhancement become stronger and more well-resolved when the concentration of the
287 paramagnetic dopant is increased (in contrast to the solid effect, which becomes less efficient
288 at high concentrations of PA).

289 Hwang and Hill provided a phenomenological description of the cross effect (CE) for systems
290 with high electron spin polarization.¹⁹ CE relies on the presence of an EPR line that is
291 inhomogeneously broadened by g-anisotropy. Such a system consists of multiple spin packets
292 with varying ESR frequencies. Consider two spin packets, 'i' and 'i+1', that are dipolar-
293 coupled, with allowed SQ EPR transition frequencies related by the expression $\omega_e^{i+1} = \omega_e^i +$
294 ω_N , where ω_N is the nuclear Larmor frequency of the nuclei that are dipolar-coupled to the
295 electron spin packets. Since $\omega_e^i + \omega_N$ is the transition frequency of the ZQ transition for the
296 spin packet *i*, this forbidden transition can now be cross coupled with the allowed SQ transition
297 of the spin packet *i+1*, ω_e^{i+1} (Figure 1c). Similarly, ω_e^i is cross-coupled to the DQ transition of
298 the spin packet *i-1*, where $\omega_e^i = \omega_e^{i-1} + \omega_N$. The resulting nuclear hyperpolarization through
299 cross-coupling of the allowed EPR transition of one spin packet with the forbidden transition
300 of another spin packet is termed the cross effect. For maximum efficiency of CE, the linewidth
301 of the inhomogeneously broadened ESR line must be greater than the nuclear Larmor
302 frequency. Because cross-coupling is possible with both DQ and ZQ transitions, lower net
303 enhancements are observed due to offsetting of positive enhancements by negative
304 enhancements.

305 **Thermal mixing:** Thermal mixing (TM) is also a three-spin process and is the dominant
306 mechanism of hyperpolarization at high concentrations of PA. TM requires high fields and
307 ultralow temperatures (< 4K), and is observed in the presence of PAs that appear to have
308 homogeneously broadened lines at low or intermediate fields but with appreciable g-factor

309 dispersion at high fields. Unlike CE (which can only yield polarization transfer between nuclei
310 with the same gyromagnetic ratio), TM allows transfer of polarization between nuclear
311 ensembles of different gyromagnetic ratios, e.g. ^1H and ^{13}C . This transfer of polarization is
312 mediated by energy transfer between different thermal spin reservoirs via dipolar interactions
313 (Figure 1c). The first mathematical description was provided by Borghini,²⁰ and a more
314 generalized mathematical description was provided by Wenckebach.²¹ First, the ESR transition
315 is saturated at frequency ω_{0S} . The central assumption in the thermal mixing mechanism is that
316 the electron spin polarization is transferred throughout the entire EPR spectrum via spin
317 diffusion, on a timescale that is much faster than any other relaxation process. This polarization
318 is then transferred to the nuclear spin reservoir through the HFI, resulting in nuclear
319 hyperpolarization.²¹

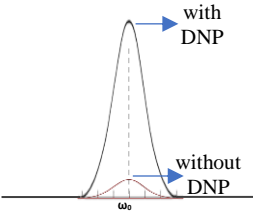
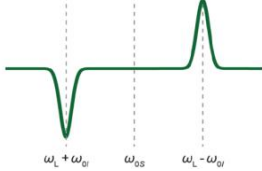
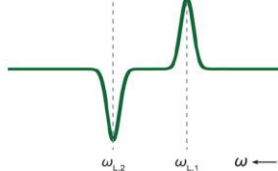
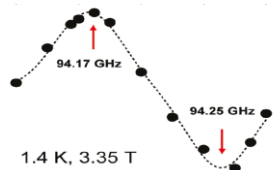
320 **Field-dependence of CE and TM:** Cross-coupling between spin packets becomes less
321 efficient at higher fields because it becomes increasingly difficult to satisfy the condition $\Delta\omega_S$
322 $> \omega_N$. Thus, both the CE and TM enhancements scale with $1/B_0$.

323 The study of solid-state nuclear hyperpolarization mechanisms is an active field, with ongoing
324 theoretical and experimental work to elucidate and quantify various factors that determine DNP
325 enhancement.²²⁻²⁴ The dominant mechanism in a DNP experiment is affected by a complex
326 interplay of experimental conditions, including temperature, field, frequency, and concentration of
327 PA.²⁵ In the solid state, more than one mechanism may be operational simultaneously. For
328 example, as the concentration of PA is increased, the SE becomes less efficient and the CE or TM
329 may take over. We have qualitatively described the origins of various mechanisms of DNP
330 enhancement, focusing on CW mechanisms which are described in terms of macroscopic rates of
331 relaxation via fluctuations of the scalar and dipolar HFI. However, we note that quantum

332 mechanical models were developed early on,^{26,27} and have also been proposed more recently for
 333 the case of EPR excitation using microwave pulses.^{28–30}

334

335 Table 1: Summary of steady-state DNP mechanisms

	Overhauser effect	Solid effect ¹	Cross-effect ¹	Thermal mixing
Typical frequency profile of DNP enhancement		Reproduced from ref. 31 with permission from the PCCP Owner Societies 	Reproduced from ref. 31 with permission from the PCCP Owner Socie 	Adapted from ref. 32 
Observed in state	Liquid	Solid	Solid	Solid
Detection schemes that apply mechanism	Direct detection, supercritical DNP	d-DNP, shuttle DNP, temperature-jump DNP, rapid-melt DNP	d-DNP, shuttle DNP, temperature-jump DNP, rapid-melt DNP	d-DNP, shuttle DNP, temperature-jump DNP, rapid-melt DNP
Interactions leading to hyperpolarization	Relaxation through contact hyperfine, dipolar hyperfine interactions. Rate of fluctuation of electron density preferentially enables DQ or ZQ transition	Level mixing through dipolar hyperfine interaction, direct excitation of DQ or ZQ transition by microwaves	Dipolar electron-electron and dipolar hyperfine interactions; inter-system cross-coupling leads to cross-polarization from electron ensemble to nuclear ensemble	Dipolar electron-electron and dipolar hyperfine interactions; spin temperatures of different nuclear ensembles are rapidly equalized via dipolar interactions, allowing heteronuclear spin hyperpolarizations
Conditions	1. Saturating SQ transition: $\omega_{mw} = \omega_{SQ}$ 2. Relaxation through either ZQ or DQ: $\omega_{motion} \approx \omega_{ZQ/DQ}$	Selective, direct excitation of either ZQ or DQ transition: $\omega_{mw} = \omega_{SQ} \pm \omega_{0l}$. Requires PA with narrow EPR linewidths to achieve selectivity of DQ or ZQ transition.	$\omega_{mw} = \omega_{SQ}$ $\Delta\omega_e \gg \omega_N$; where $\Delta\omega_e$ is the width of the inhomogeneously broadened EPR line	$\omega_{mw} = \omega_{SQ}$ $\Delta\omega_e \gg \omega_N$; where $\Delta\omega_e$ is the width of the inhomogeneously broadened EPR line

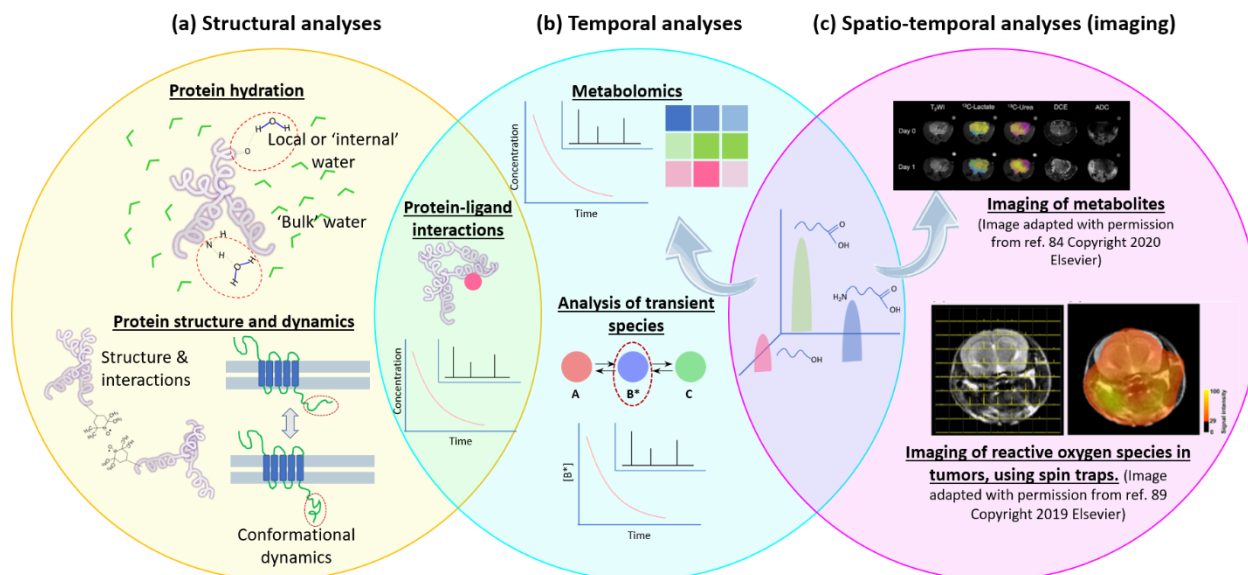
336 ¹B. Corzilius, *Phys. Chem. Chem. Phys.*, 2016, **18**, 27190 - Published by the PCCP Owner Societies

337

338

339 **Section II: Applications of liquid-state DNP NMR**

340



341

342 **Figure 2:** Overview of current and potential future applications of liquid-state DNP NMR. (a)
343 Increasing the sensitivity of spectroscopic applications for structural studies; (b) Spectroscopic
344 identification of transient species such as reaction intermediates in solution; (c) Imaging of species
345 with low steady-state concentrations, e.g., metabolites and free radicals at ambient temperature.
346 The overlapping areas of the three circles show applications that combine different types of studies.

347 The examples listed below and summarized in Figure 2 show that liquid-state DNP NMR has

348 broad and fundamental applications ranging from studies of reaction kinetics and mechanisms,

349 metabolomics, imaging/metabolic imaging, to structural studies of biomolecules. Liquid-state

350 DNP NMR is also envisioned to have a profound impact on the future of quantitative NMR.³³ Here

351 we note some areas where liquid-state DNP NMR has yielded or promises to yield unique,

352 previously unavailable information.

353 ➤ **Studying protein hydration:** Liquid-state NMR studies provide information about dynamics

354 of solute-solvent interactions. For example, protein molecules are surrounded by a hydration

355 layer, the dynamics and heterogeneity of which are thought to be a determinant of protein

356 function.³⁴ Han *et al.* have conducted seminal work in the use of Overhauser DNP (ODNP) for

357 selective probing of local or 'internal' water surrounding peptides and proteins in varied

358 environments.³⁵⁻³⁷ Using a combination of site-directed spin-labeling and ODNP, Han *et al.*
359 separate signals of local water surrounding a protein from bulk aqueous solution. In this
360 method, DNP occurs by transfer of electron spin polarization of spin labels attached at selected
361 sites to protons of water molecules diffusing in the vicinity of the spin label. Translational
362 diffusion of the water molecules modulates the dipolar interaction between the electron spin
363 of the spin label and nuclear spins of the local water protons, and this modulation results in
364 cross-polarization from the electron spins to the nuclear spins through the Overhauser effect.
365 Thus, ODNP isolates the translational dynamics of the hydration layer, occurring on the
366 picosecond-to-nanosecond timescale. Secondly, ODNP selectively amplifies the signal from
367 water molecules interacting with the site of interest, while separating out the background NMR
368 signal of bulk water. More recently, the technique has been used by Segawa *et al.* to observe
369 penetration of water into a model membrane and its interaction with a membrane-inserting
370 peptide.³⁸ They found that ODNP was the only technique able to distinguish accessibility in a
371 site-selective manner, validating the utility of ODNP in distinguishing areas of heterogeneity
372 with single-residue resolution. Chaubey *et al.* observed changes in dynamics of the solvent
373 2,2,2-trifluoroethanol (TFE) when the peptide melittin undergoes structural reorganization
374 from a random coil to a helical structure. They measured the DNP enhancement of ¹⁹F by the
375 polarizing agent TEMPOL, and used the DNP coupling parameter as an indicator of the
376 correlation time of the co-solvent TFE.³⁹ Hyperpolarized water has also been used to measure
377 protein hydration by increasing the sensitivity of techniques such as fast 2D NMR, exchange
378 spectroscopy (EXSY), and nuclear Overhauser effect spectroscopy (NOESY).⁴⁰⁻⁴³

379 **Studying membrane proteins, disordered proteins, and aggregation-prone**
380 **biomacromolecular systems:** Membrane proteins are a particularly suitable example of the type

381 of aggregation-prone biomacromolecules that could benefit from improvements to liquid-state
382 DNP NMR. The maturation of solid-state DNP NMR with MAS has yielded valuable high-
383 resolution structural information about these systems.^{44,45} However, these proteins remain difficult
384 to solubilize/reconstitute in active form.² Liquid DNP NMR can provide information about
385 dynamics processes, such as changes in conformation and solvation, for a wide range of samples,
386 including in-cell samples. An advantage of DNP NMR is that by using site-directed spin labeling,
387 hyperpolarization can be achieved with high site-specificity, thus allowing highly localized
388 probing of protein dynamics and secondary structure. Hilty *et al.* recently used the method of
389 dissolution-DNP (d-DNP) to hyperpolarize lipids (dodecyl phosphocholine), and monitored lipid
390 interactions with the membrane protein OmpX.⁴⁶ By exploiting the facile exchange of amide
391 protons, hyperpolarized water has also been used to obtain high-resolution 2D NMR spectra of
392 disordered proteins.⁴⁷ Hyperpolarized ligands have been used to selectively enhance signals of
393 ligand-binding sites^{48,49} or to transfer polarization to other nearby ligands⁵⁰ on the protein. A
394 potential application of high-throughput, quantitative analysis of ligand-protein interactions using
395 liquid-state DNP NMR is the screening of small-molecule ligands for drug development.^{48,51}
396 (High-throughput biochemical assays, typically based on fluorescence readout, are the workhorses
397 to identify potential drug/target combinations; however, such assays do not provide the atomic-
398 level structural details required for *in silico* methods for drug design and discovery.⁵²)

399 ➤ **Observing transiently formed species in solution for reaction monitoring and mechanistic**
400 **studies.** Hyperpolarization amplifies the NMR signal so that single-scan pulse experiments
401 with otherwise low sensitivity can now be used to track the progress of a reaction by monitoring
402 temporal profiles of NMR spectra. This ability has been used to observe reaction intermediates,
403 conduct mechanistic studies, and monitor reaction kinetics.

404 Hilty *et al.* have conducted extensive work on the use of hyperpolarized substrates for
405 monitoring non-equilibrium reactions with second to sub-second resolution.^{53,54} Recently, they
406 used d-DNP-enhanced pulse NMR to monitor the styrene polymerization reaction and the
407 reaction of *p*-anisaldehyde with isobutylamine, with second-scale resolution.⁵⁵ They were able
408 to extract single-scan ¹H-¹³C correlation spectra during the reaction and calculated ¹H chemical
409 shifts from ¹³C spectra of transient species, demonstrating direct observation of transient
410 species formed during the reaction. Jensen and Meier used hyperpolarized fructose to identify
411 a previously elusive reaction intermediate and to monitor the carbohydrate dehydration
412 reaction.⁵⁶ There are many examples of the use of d-DNP to identify reaction intermediates
413 and measure reaction kinetics of organic and inorganic reactions.⁵⁷⁻⁶¹

414 Hyperpolarization has been similarly exploited to study kinetics of protein-enzyme/protein-
415 ligand complex formation. ¹³C NMR spectra provide signatures of protein-ligand binding, and
416 the broad frequency dispersion of ¹³C spectra overcomes the problem of potential chemical
417 shift overlap encountered in proton NMR. However, ¹³C NMR spectra are weaker than ¹H
418 NMR spectra because of the lower gyromagnetic ratio of ¹³C. DNP enhances the weak ¹³C
419 signals, and has been used for ligand binding studies, including enzymatic assays.⁶² As with
420 organic reactions, d-DNP has been used to increase the signal intensity of single-scan ¹³C
421 spectra collected when monitoring biochemical reactions, enabling acquisition of data points
422 at sub-second intervals for more than a minute as the reaction progresses.⁶³⁻⁶⁷ Hilty *et al.* have
423 used DNP to obtain ¹³C DNP NMR spectra of lipid membranes, characterizing their
424 biosynthetic pathways based on fractional isotopic labeling of reactant feeds.⁶⁸ Duus *et al.* also
425 used DNP of ¹³C to study the mechanism and kinetics of transglycosylation.⁶⁹

426 ➤ **Metabolomics:** NMR of heteronuclei (nuclei other than ^1H , e.g. ^{13}C , ^{15}N etc.) is advantageous
427 for metabolite profiling because the NMR signals of heteronuclei are dispersed over a large
428 frequency range and also do not need to be separated from the large background signal of
429 aqueous protons in cells. However, the low, shifting concentrations of metabolites along with
430 the low natural abundances of NMR-active heteronuclei result in metabolite quantities that are
431 undetectable by conventional NMR spectroscopy. Hyperpolarization can amplify the signal
432 from these low-concentration metabolites and increase the speed of analysis by eliminating the
433 need for signal averaging. The increased signal-to-noise ratio (SNR) and speed of data
434 collection allow real-time detection and monitoring of metabolites for clinical and investigative
435 purposes. This approach was first demonstrated by Thaning *et al.*, who injected ^{13}C -
436 hyperpolarized pyruvate into rats, and subsequently detected, monitored, and quantified the
437 metabolites lactate, hydrate, alanine, bicarbonate, and pyruvate at 3 s intervals for 50 s after
438 injection.⁷⁰ Ardenkjær-Larsen *et al.* demonstrated the utility of ^{13}C d-DNP NMR to determine
439 levels of the anticonvulsant carbamazepine and its major metabolite carbamazepine-10,11-
440 epoxide in blood plasma.⁷¹ Brindle *et al.* conducted *in vitro* and *in vivo* studies of ascorbic and
441 dehydroascorbic acid hyperpolarized by d-DNP, using these as probes of tumor redox status
442 (loosely understood as the balance of oxidants and anti-oxidants in cells).⁷² The signal
443 intensities of metabolites tracked in these reports indicate the suitability of DNP NMR for
444 quantitative NMR.⁷³

445 ➤ **In-cell DNP NMR:** All the above-mentioned analyses, including reaction monitoring and
446 metabolite analyses, can provide valuable information if conducted within a native cellular
447 environment. Frydman *et al.* used d-DNP followed by magnetization transfer from ^{13}C to ^1H
448 to monitor the actions of pyruvate decarboxylase and pyruvate formase lyase enzymes.⁷⁴ They

449 were able to perform these experiments in both yeast and bacteria. Meier *et al.* observed acetate
450 influx and subsequent metabolic consequences in yeast.⁷⁵ Meier *et al.* and Balbach *et al.* have
451 presented comprehensive reviews of the applications of in-cell hyperpolarized NMR.^{76, 77} It
452 should be noted that solid-state in-cell DNP NMR is an emerging field.^{78,79} However, only
453 liquid-state DNP has the potential to provide information about dynamic processes such as
454 conformational changes, reaction kinetics and evolution of metabolite profiles in intact cells.

455 ➤ **Imaging/Metabolic imaging:** In addition to spectroscopic metabolite profiling,
456 hyperpolarization also improves imaging of metabolites by amplifying their NMR signal.⁷⁰
457 ¹³C-labeled pyruvate is the most commonly used molecular probe in metabolic imaging, which
458 is expected to be highly impactful as a clinical tool because of the noninvasive nature of
459 magnetic resonance techniques and non-toxicity of spin-probes,^{80,81} many of which occur
460 endogenously. Metabolic imaging of hyperpolarized pyruvate is expected to be useful for
461 tracking redox status of tissues, oxidative stress, and profiling the effects of radiation.⁸²⁻⁸⁴
462 Similar to the study by Thaning *et al.*, Ardenkjaer-Larsen *et al.* demonstrated the use of
463 metabolic imaging to scan implanted tumors in rats and to quantify the glycolytic status of
464 cancer cells.⁸⁵ Glycolysis has also been quantified by imaging of hyperpolarized ¹³C-labeled
465 glucose⁸⁶ and fructose.⁸⁷

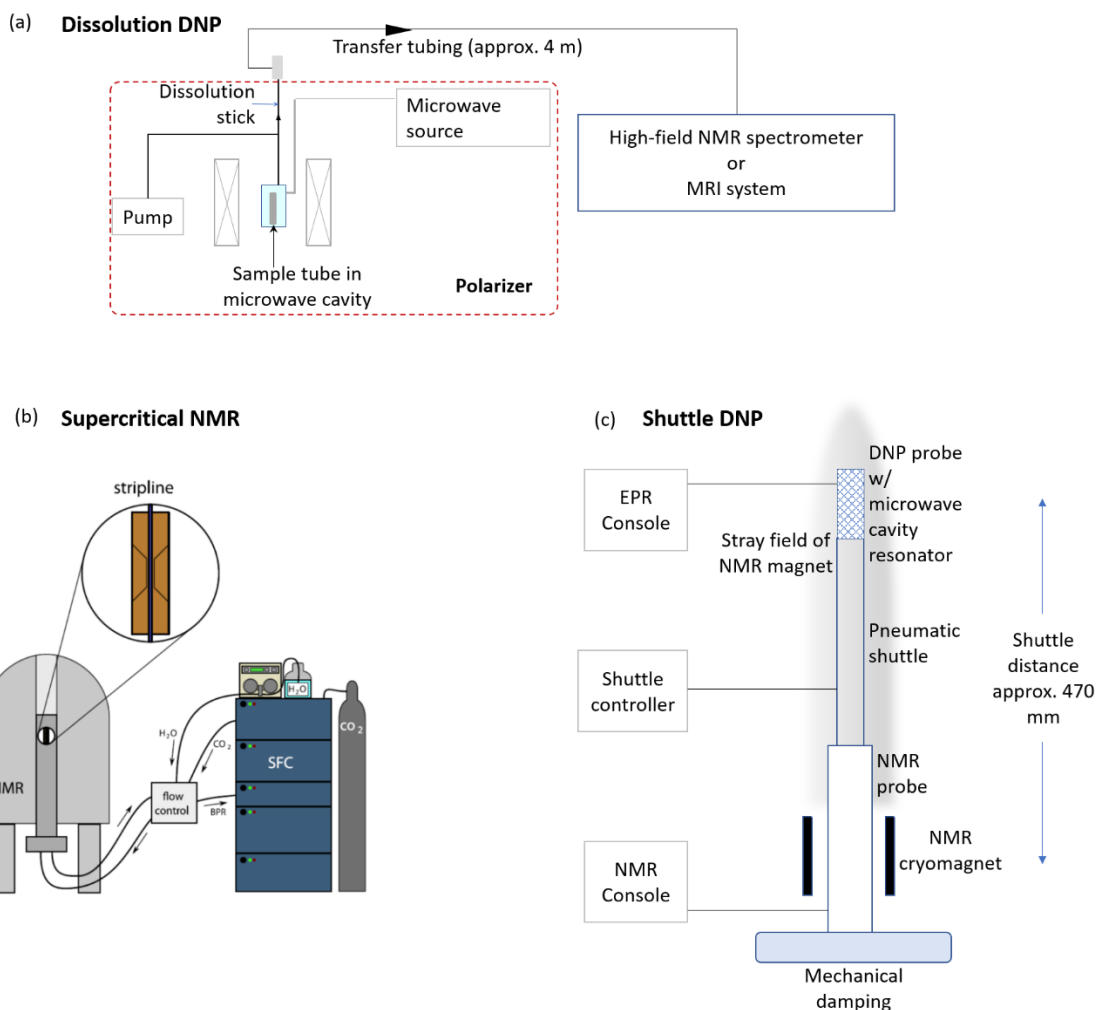
466 Hyperpolarization enhancements can be similarly used to image other types of spin probes and
467 spin traps. ¹³C-labeled spin traps have been used to image reactive oxygen species (ROS) in
468 tumors, allowing quantification of the redox status of cancer cells. When the hyperpolarized
469 spin-trap is injected into the tumor, it reacts with ROS to form diamagnetic adducts.
470 Hyperpolarization allows detection of reaction intermediates, which is the origin of the
471 measured signal prior to adduct formation.^{88,89}

472 ➤ **Increasing the sensitivity of alternative NMR methodologies and low-field NMR:** In NMR
473 relaxometry, sample components are characterized by their magnetization decay profiles (due
474 to spin-lattice relaxation or spin decoherence) as a function of field or frequency. This
475 technique suffers from poor sensitivity and resolution at lower frequencies and in multi-
476 component chemical systems. Hyperpolarization via a spin label can enhance the signal at low
477 frequencies while also allowing observation of specific sites via DNP through spin labels. DNP
478 enhanced NMR can be used as a complementary technique to relaxometry,⁹⁰ but DNP may
479 also be used to enhance signals for relaxometry. Selective DNP-enhanced fast field cycling
480 (FFC) relaxometry can be used to separate signals of protein and solvent⁹¹ or to measure the
481 properties of the composing polymers of a block copolymer in solution.⁹² Finally, relaxometry
482 profiles in the solution state can help to design ODNP material systems by predicting DNP
483 enhancements.^{93,94} Low-field NMR, which has particular applications in compact NMR and *in*
484 *vivo* imaging, is another sub-field in which gains of more than a hundred-fold may be obtained
485 by using DNP. Compact NMR can enable ‘on-field’ measurements of low-concentration
486 analytes, including hazardous substances and reaction intermediates.⁹⁵⁻⁹⁷ Increasing the
487 sensitivity of low-field magnetic resonance imaging would be highly beneficial for developing
488 low-cost *in vivo* imaging instruments that do not require cryogenics, which are increasingly
489 scarce.^{98,99}

490 **Section III: Available detection schemes and challenges for liquid-state samples**

491 **Detection schemes:** Of the DNP mechanisms discussed above, only the Overhauser effect is
492 applicable directly to liquid-state samples. However, there are several experimental challenges
493 associated with this mechanism, including lower efficiency at higher fields, solvent heating effects
494 due to the high microwave power required to saturate the ESR transition, and lack of applicability

495 to large molecules (this point is especially relevant for biomacromolecular samples). Low
496 temperatures favor high enhancement factors, which is likely why early successes in detection
497 schemes for liquid samples involved melting frozen solutions; hyperpolarization is achieved in the
498 frozen, solid state at low or intermediate fields. The sample is then melted or rapidly dissolved in
499 a hot solvent and transported to another high-field location, where NMR spectroscopy is conducted
500 on the melted sample (or imaging conducted of the liquid sample injected into tissue). Such *ex situ*
501 detection schemes have been highly successful for enhancing the NMR signals of liquid samples.
502 Challenges associated with *ex situ* hyperpolarization are: (i) loss of polarization during transport
503 and (ii) inability to average over multiple scans because sample preparation requires several hours
504 and the sample is lost after one cycle due to dissolution in the hot solvent. On the other hand, *in*
505 *situ* detection schemes eliminate the transport step, conduct DNP and NMR at the same field, and
506 allow averaging over multiple scans. Prominent *ex situ* and *in situ* schemes are summarized below.
507



508
 509 **Figure 3:** Summary of *ex situ* detection schemes. (a) Main components of a d-DNP setup. (b)
 510 Schematic of a supercritical NMR setup, which can be adapted for DNP by the addition of a
 511 microwave source and resonator. (Adapted with permission from ref. 100 Copyright 2016
 512 Elsevier) (c) Main components of a shuttle-DNP setup.

513 **1. *Ex situ* detection:** As mentioned above, the experimental conditions (low temperatures and
514 low-to-medium fields) that favor DNP are incompatible with those that are desirable for NMR
515 spectroscopy of liquids (high fields that provide better sensitivity and resolution, and
516 temperatures near room temperature). *Ex situ* methods overcome this incompatibility by
517 separating the DNP and NMR steps so that each step is conducted under its respective optimal
518 conditions. DNP is conducted in a separate location (either a separate magnet or the stray-field
519 region of the NMR magnet) at lower fields and low temperature (in the frozen state). The
520 hyperpolarized sample is then rapidly melted or dissolved in a hot solvent and transported to a
521 separate high-field location where NMR spectroscopy is carried out. Here we label *ex situ*
522 methods as all those in which there is a separation of locations for DNP and subsequent NMR
523 detection. These locations may be separated by as little as a few cm or the sample may be
524 transported to a completely different instrumental unit.

525 **1.1. Dissolution DNP:** Dissolution DNP (d-DNP)¹⁵ is perhaps the most impactful
526 hyperpolarization scheme implemented thus far, with commercial setups available
527 (Hypersense by Oxford Instruments and SPINlab by GE Healthcare[†]) and several ‘home-
528 made’ setups reported.^{102–108}

529

530

[†]Certain commercial entities, equipment or materials may be identified in this document to describe an experimental procedure or concept adequately. Such identification is not intended to imply recommendation or endorsement by the National Institute of Standards and Technology, nor is it intended to imply that the entities, materials or equipment are necessarily the best available for the purpose.

531 Ardenkjær-Larsen *et al.* showed that hyperpolarization of a frozen solution (achieved via
532 a solid-state mechanism i.e. solid effect, cross effect, or thermal mixing) is stable enough
533 to be detected if the frozen solution is melted rapidly by dissolution in a hot solvent.¹⁵
534 After the sample has been hyperpolarized, it is transported to a separate location for either
535 spectroscopy¹⁵ or imaging¹⁰⁹, provided the transport is accomplished more quickly than
536 the relaxation of the sample polarization.

537 In d-DNP, hyperpolarization is carried out in the ‘polarizer’ (consisting of the magnet and
538 cryostat) at a temperature of 1 K and static magnetic fields in the range of 3 T to 7 T. The
539 optimal field for d-DNP depends on the relative relaxation times of nuclear and electron
540 spin polarizations. Higher fields result in longer nuclear relaxation times while maintaining
541 rapid electron-spin relaxation. Thus, d-DNP typically employs medium-to-high static
542 magnetic fields, and future setups are projected to work with even higher fields.¹¹⁰ A
543 paramagnetic material with a narrow EPR line – typically a trityl or nitroxide radical – is
544 dissolved in glycerol to a concentration of 10 mmol L⁻¹ to 20 mmol L⁻¹. When frozen, this
545 solution forms a glassy, homogeneously doped paramagnetic matrix that hyperpolarizes
546 the nuclear spin ensemble of the sample. Hyperpolarization can also be achieved by first
547 transferring polarization from unpaired electrons to protons, followed by cross-polarization
548 to other low- γ nuclei, e.g. ¹H-¹³C cross-polarization. A low-quality-factor (low- Q) metal
549 cylinder is used to localize microwaves around the sample. Saddle coils fitted inside the
550 metal cylinder are used to conduct solid-state NMR measurements of hyperpolarization
551 while the sample is still in the polarizer. After hyperpolarization, superheated water is
552 rapidly injected into the frozen glassy sample to convert it to an aqueous solution, which
553 is transported out of the low-temperature region and either used for NMR spectroscopy at

554 a higher field ($> 9 \text{ T}$)¹⁵ or injected into a tissue sample for imaging *in vitro* or *in vivo*.¹⁰⁹
555 The sample volume is typically around $100 \mu\text{L}$ and the volume of injected solvent is
556 typically around 5 mL , resulting in dilution. Polarizations of 30% to 90% have been
557 reported, translating to improvements of up to four orders of magnitude in the SNR,
558 compared to NMR without DNP.

559 DNP requires high microwave powers in order to saturate the EPR transition. In d-DNP,
560 high-power sources, such as gyrotrons with typical power outputs of approximately 200
561 mW are used to generate microwaves. Saturation of broad EPR lines can be improved by
562 modulating the microwave frequency or field, which increases the fraction of DNP-active
563 radicals.^{111,112} Next, it is critical to transport the hyperpolarized sample to its destination
564 without significant loss of polarization, which is exacerbated by the presence of the
565 paramagnetic material acting as a relaxant of nuclear spin polarization. The transport step
566 is automated so it can be accomplished within a few seconds.¹¹³ Fields of a few tenths of a
567 mT applied while transporting the sample are usually adequate to preserve polarization.¹¹⁴

568 d-DNP is most advantageous for inherently *ex situ* applications, e.g., it has been highly
569 impactful by improving signals for *in vivo* imaging and it also enables real-time monitoring
570 of metabolites.^{70,86} However, it is limited by the long time – often several hours – required
571 to generate the hyperpolarized sample, which must then be transported and measured
572 before the nuclear polarization relaxes. Widespread application of d-DNP in clinical
573 settings requires that hyperpolarization be accomplished on large sample volumes (e.g.
574 through high throughput) in a consistent and reproducible manner (quality control). To
575 achieve these objectives, the following improvements have either been reported or are
576 expected: (i) magnet design (incorporation of shielded magnets and dual-core magnets in

577 the polarizer so that NMR spectroscopy can be conducted after short transport); (ii)
578 development of optimized high- Q microwave resonators for greater saturation of the EPR
579 transition; (iii) improvements in transport systems, e.g., the use of pneumatic systems to
580 speed up transport from a timescale of several seconds to less than a second;¹¹⁵ (iv)
581 development of labile radicals or radical-free phases to eliminate paramagnetic species and
582 extend the relaxation time of nuclear polarization; or formulation of persistent,
583 transportable hyperpolarized states by manipulation of multi-phase systems.^{116,117}

584 **1.2. Supercritical DNP:** When Overhauser enhancement occurs through e-n cross-relaxation
585 mediated by the dipolar component of the HFI, the frequency of modulation of the dipolar
586 interaction must match the energy gaps associated with the forbidden transitions. These
587 energy gaps increase at higher fields, and the correlation times must be correspondingly
588 shorter to provide the required high-frequency modulation of the HFI. (This trend may not
589 apply when the HFI is dominated by the scalar component, whose magnitude is
590 independent of field.) Fast molecular motions in supercritical fluids result in
591 correspondingly short correlation times and therefore, improved Overhauser
592 enhancements.^{16,118} Supercritical CO₂ can be obtained under relatively mild conditions –
593 at room temperature and a pressure of approximately 7500 kPa. In supercritical DNP
594 NMR, DNP is carried out at a lower field of 0.3 T. The supercritical solution is then
595 transported to the high-field NMR magnet using a flow system.

596 Building on their work on flow-transfer NMR,¹¹⁹⁻¹²¹ Dorn *et al.* have established the use
597 of supercritical solvents for flow-transfer DNP NMR.¹⁶ They use two protocols for flow
598 DNP NMR: liquid-liquid intermolecular transfer (LLIT)¹¹⁹ and solid-liquid intermolecular
599 transfer (SLIT).^{120,121} In the setup for LLIT, the solution is pumped from a high

600 performance liquid chromatography (HPLC) unit, mixed with analytical grade CO₂
601 pumped from a superfluid chromatography unit (SFU), and equilibrated to a pressure of
602 17000 kPa (165 atm). The volume ratios of sample solution and CO₂ are determined by
603 their relative flow rates. Thus, a 0.1 mL/min flow of sample solution and 1 mL/min flow
604 of CO₂ at the time of mixing results in a 1:10 ratio of sample volume to supercritical CO₂
605 volume for hyperpolarization. The mixture is heated to 40 °C in a superfluid
606 chromatography (SFC) oven, and the resulting supercritical fluid is directed to a low-field
607 (0.33 T) magnet where hyperpolarization is carried out. Microwaves are generated by a
608 klystron source, amplified, and localized at the sample volume using a TE102 cavity
609 resonator. The hyperpolarized solution is then flowed to a high-field magnet for NMR
610 spectroscopy. Here, radiowaves are localized at the sample volume using a Helmholtz
611 detection coil. The typical sample volume is approximately 160 μL in the low-field magnet
612 and approximately 60 μL in the high-field magnet.

613 The protocol for DNP NMR using SLIT is identical to the LLIT protocol, except that the
614 sample flowing from the HPLC unit through the SFC oven does not contain the PA, i.e.
615 nitroxide radicals. Nitroxide radicals immobilized on silica gel are placed in the 0.3 T
616 magnet and hyperpolarization occurs as the supercritical solution flows over the silica gel.
617 For benzene, Dorn *et al.* reported approximately 5-fold improvement of observed DNP
618 enhancement in LLIT using supercritical CO₂ when compared to ‘normal-flow’ DNP
619 NMR. SLIT DNP NMR with supercritical CO₂ showed a 10-fold improvement in
620 observed DNP enhancement compared to normal-flow DNP NMR. In addition to better
621 sensitivity, SLIT separates the PA from the sample and thus avoids the problem of
622 paramagnetic relaxation during transfer from the low-field magnet to the high-field

623 magnet. Finally, since the paramagnetic material is not mixed with the sample in the SLIT
624 protocol, the sample can be recycled for multiple measurements.

625 Supercritical CO₂ has several desirable properties that make supercritical DNP a
626 promising methodology, particularly for small-molecule analytes.^{7,85} The polarity of
627 supercritical CO₂ can be varied continuously by adding small volumes of co-solvents,
628 making it suitable for polar as well as non-polar solutes. CO₂ is non-polar and thus avoids
629 the dielectric heating effects observed in solvents like water. This is particularly important
630 considering the high intensity of microwaves typically required for DNP. The use of CO₂
631 as a solvent yields a proton-free background. Most importantly, supercritical DNP gives
632 the ability to achieve fast molecular tumbling, achieving correlation times of 2 ps to 5 ps
633 at room temperature (compared to 5 ps to 6 ps at 400 K for water). These fast correlation
634 times can enable Overhauser DNP at correspondingly higher fields/frequencies, making
635 supercritical DNP an exciting prospect for enabling direct DNP enhancement in high-field
636 NMR.

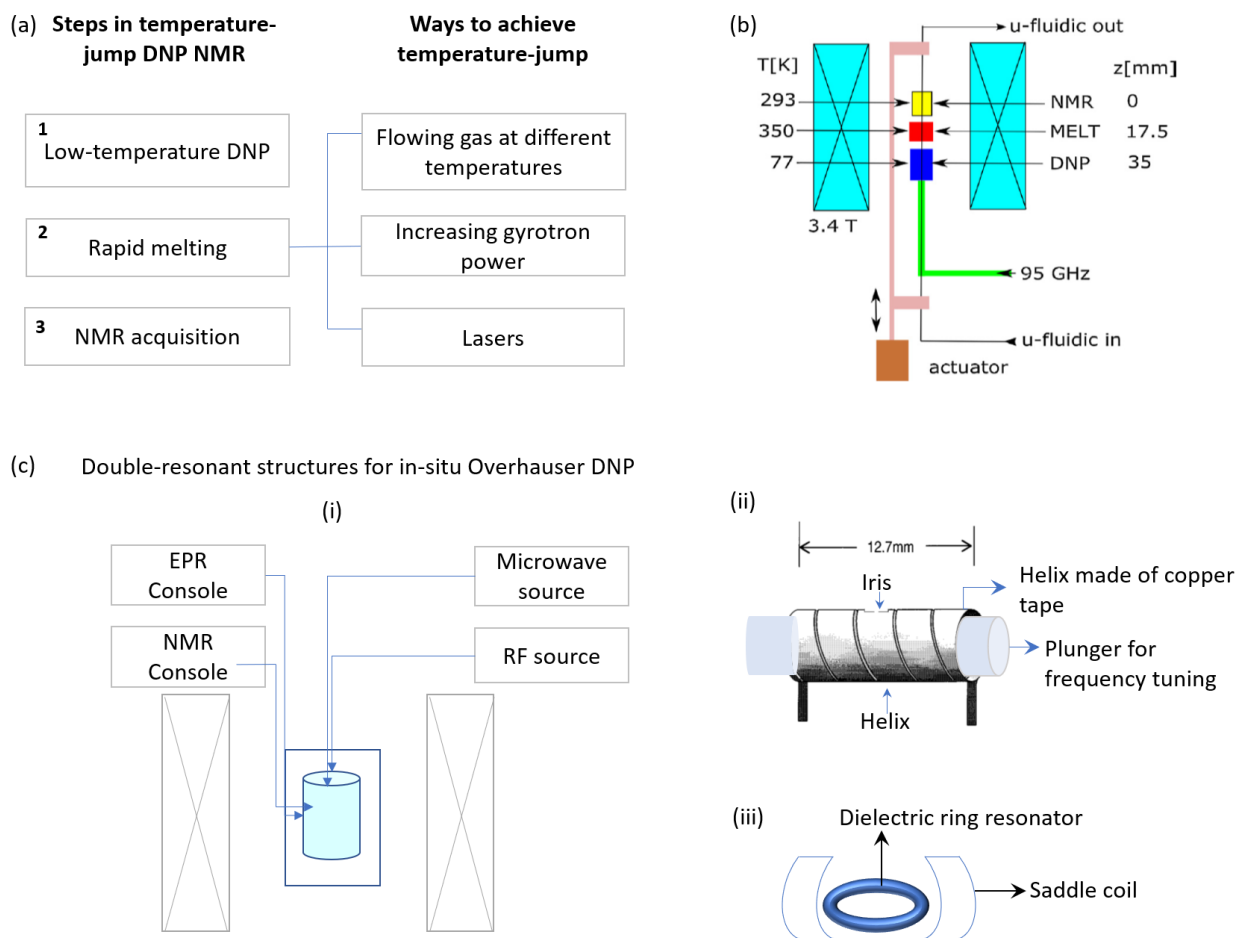
637 **1.3. Shuttle DNP:** In shuttle DNP, the probe containing the liquid sample is shuttled between
638 the low-field and high-field region produced by the same magnet, allowing separation of
639 hyperpolarization and detection steps. Hyperpolarization occurs through Overhauser
640 enhancement at low magnetic fields, after which the sample is shuttled to the high-field
641 region for NMR detection. There are many early examples of the use of setups with
642 multiple magnetic field regions in zero-field NMR, low-field NMR, NMR relaxation, and
643 relaxation-dispersion measurements, which form the basis of the instrumental setups used
644 in shuttle DNP.¹²²⁻¹²⁴ In such setups, it is desirable to have several magnetic field regions
645 either to separate the relaxation and detection steps or to study the field-dependence of

646 relaxation time. Typically, the liquid sample is shuttled by a computerized pneumatic
647 system over distances of 10 cm to 100 cm in times < 1 s. Fast and precise positioning at
648 locations of specific field strengths in the fringe field of a magnet can be accomplished
649 using stepper motors. Such setups have been used for fast field cycling NMR and the
650 application has been extended to chemically-induced DNP (CIDNP) experiments.^{125,126}

651 In the liquid state, there can be many reasons (besides inverse field-dependence of
652 Overhauser enhancement) for choosing to conduct DNP at a lower field than that used for
653 NMR detection. For example, Reese *et al.* chose to conduct hyperpolarization at the lower
654 frequency of 10 GHz (0.3 T) because the larger wavelength allows higher sample sizes and
655 decreased dielectric losses in an optimally designed cylindrical resonant cavity.¹²⁷ After
656 DNP, the sample is shuttled downwards pneumatically to a 14 T magnet to take advantage
657 of the higher sensitivity and resolution of high-field NMR detection. This setup is not
658 efficient for large molecules with fast proton relaxation times because hyperpolarization
659 cannot be sustained through the drop in magnetic field during the shuttling step. In a
660 variation of this setup, the low-field region is located in the stray field of the 14 T NMR
661 magnet.¹²⁸ A ferromagnetic cylinder used for shimming provides a homogeneous-field
662 length of 10 mm. By avoiding the drop in magnetization during a long transfer to a separate
663 magnet, this setup extends the scope of shuttle DNP NMR to larger molecules.

664 **2. *In situ* detection:** Several ways have been proposed to overcome the problem of loss of
665 polarization during sample transport, including two-center magnets and magnetic tubes. On
666 the other hand, so-called '*in situ*' methods aim to eliminate sample transport altogether by
667 carrying out DNP and NMR at the same magnetic field. Disadvantages of DNP NMR in the
668 liquid state are the lower efficiency of the Overhauser effect at higher fields and excessive

669 heating of polar solvents such as water due to application of high-intensity microwaves.
 670 Nonetheless, *in situ* methods promise sample recyclability and greater retention of polarization
 671 before NMR detection, which also leads to greater concentration sensitivity. Here we cover the
 672 main classes of protocols for *in situ* DNP NMR. Of these, temperature-jump and rapid-melt
 673 DNP NMR work by achieving hyperpolarization in the frozen state, followed by detection in
 674 the melted state. Lastly, we discuss the experimental developments that have enabled direct *in*
 675 *situ* Overhauser DNP in the liquid state, followed by NMR detection without any intervening
 676 steps.



677

678 **Figure 4:** Summary of *in situ* detection schemes. (a) Schematic of steps in temperature-jump
679 NMR. The temperature can be produced using gas flow, microwave power from a gyrotron, or
680 lasers. (b) Schematic of a rapid-melt apparatus consisting of microfluidic channels. Adapted with
681 permission from ref. 101 Copyright 2015 Elsevier (c) i. Schematic of an *in situ* Overhauser setup
682 where both DNP and NMR are conducted at the same magnetic field. To increase B_1 intensity,
683 double resonant structures are used, for example: ii. a double-resonant flat helical cylinder (adapted
684 with permission from *Weis et al. J. Magn. Res.* **140**, 293-299 Copyright 1999 Academic Press) or
685 iii. a cylindrical resonator with matched ENDOR coils.
686

687 **2.1. Temperature jump DNP NMR:** One way of eliminating the transport step of *ex situ*
688 techniques is by conducting DNP and NMR in the same magnet. DNP is conducted at low
689 temperatures, after which the sample is rapidly melted *in situ* for NMR spectroscopy. The
690 first example of such an implementation was by Akasaka *et al.*, who achieved the
691 temperature jump using gas flowed through valves placed adjacent to the NMR probe.¹²⁹
692 In the *in situ* DNP NMR apparatus implemented by the Griffin lab, the temperature jump
693 is effected using an infrared pulse.^{130,131} To overcome the lower Overhauser enhancements
694 at higher fields, Griffin *et al.* use cross-polarization pulse sequences to transfer
695 polarization from ^1H to low- γ nuclei such as ^{13}C or ^{15}N .¹³⁰ They have also reported direct
696 detection of ^{13}C using total correlated spectroscopy (TOCSY).¹³¹ In these experiments, the
697 sample is cooled to 90 K or 100 K, hyperpolarized, melted rapidly using a CO_2 laser, and
698 then subjected to NMR experiments. 10 μL of the sample is placed in a 2.5 mm o.d. quartz
699 tube and the laser beam directed to the sample using an optical fiber. A gyrotron provides
700 high-intensity continuous microwave irradiation required for DNP. The Kockenberger
701 group have reported an improvement to this setup by conducting DNP at liquid-helium
702 temperatures and using a high-power erbium-doped yttrium aluminium garnet (Er: YAG)
703 laser for rapid melting of the sample.¹³² Recently, Yoon *et al.* have reported the use of a
704 frequency-tunable and power-tunable gyrotron that can be used for both DNP and melting

705 steps. DNP is carried out using a microwave power of 1 W to 5 W, following which a
706 high-power (> 50 W) microwave pulse is applied to melt the sample in < 1 s.¹³³ The sample
707 is placed in a saddle coil for application of radiowaves, while microwaves are applied
708 without the use of a resonator.

709 **2.2. Rapid-melt DNP NMR:** van Bentum's group have developed an *in situ* apparatus that
710 works for mass-limited samples (10 nL to 1 μ L), in which the sample is contained in a
711 microfluidic capillary.¹⁰¹ The capillary is placed on a microstrip probe that provides
712 radiofrequency (RF) excitation for NMR spectroscopy. The capillary and microstrip are
713 placed in a microwave cavity that can work in either resonant or non-resonant mode.
714 Similar to the temperature-jump apparatus by Akasaka *et al.*,¹²⁹ this apparatus also uses
715 gas flow to control the sample temperature. In van Bentum *et al.*'s apparatus, channels for
716 liquid nitrogen and warm nitrogen gas (equally applicable to liquid helium) are fabricated
717 in a poly(methyl methacrylate) (PMMA) block molded around the microwave cavity to
718 enable rapid freezing and melting of the sample as it is moved over a distance of < 5 cm
719 in this region of highest magnetic field homogeneity. Three separate regions are delineated
720 within this range: a 77 K region for DNP, a 350 K region for melting and a 300 K region
721 for NMR spectroscopy. An actuator moves the capillary between these regions, whose
722 temperature is controlled by the flow of liquid nitrogen. DNP and NMR are carried out at
723 the same magnetic field, making this an *in situ* detection protocol. DNP is carried out in
724 the frozen solid state while NMR detection can be carried out either in the liquid state or
725 in the frozen state. The small volume and ability for rapid melting/freezing eliminate the
726 time required for sample preparation and repeatability of the melt-freeze cycle enables

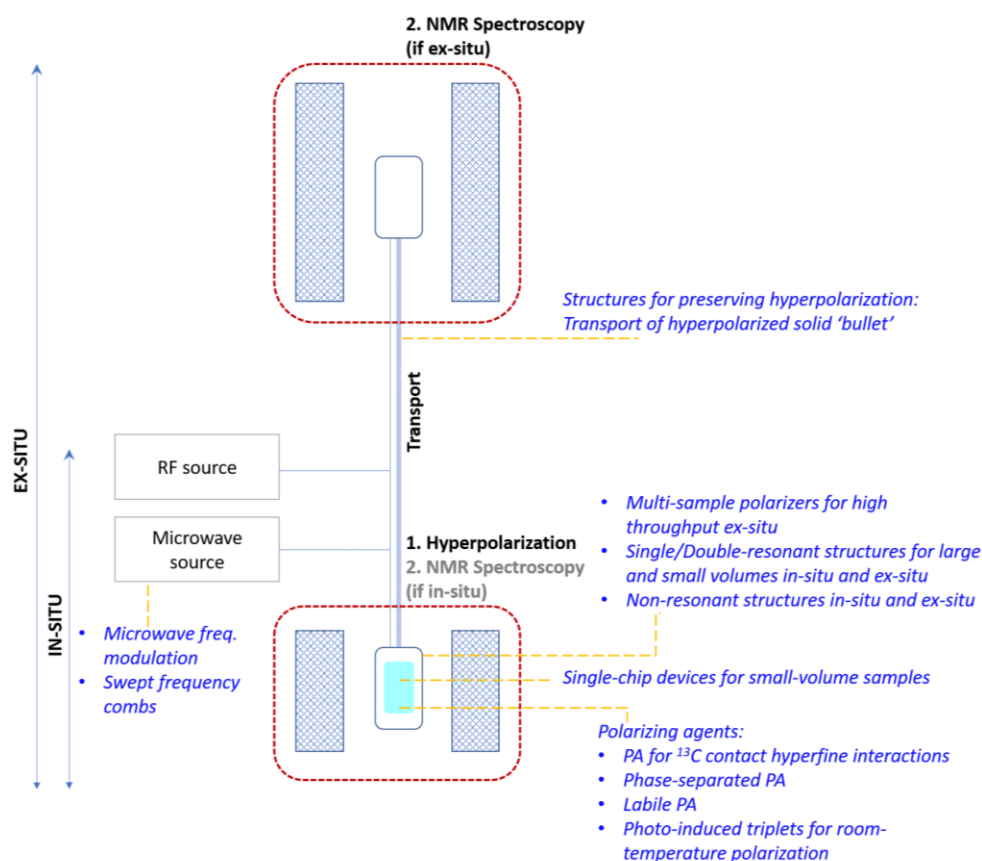
727 averaging over multiple scans. van Meerten *et al.* have demonstrated the implementation
728 of this apparatus for high-frequency, multinuclear NMR experiments.¹³⁴

729 **2.3. *In situ* Overhauser DNP:** While the above-mentioned *in situ* schemes provide
730 improvements for spectroscopic measurements of small molecules, direct Overhauser
731 enhancement would extend the benefits of hyperpolarization to larger molecules and
732 biomacromolecular systems. The Prisner group and the Bennati group showed that direct
733 Overhauser DNP enhancements for liquids at high magnetic fields can be larger than
734 expected due to contributions from scalar HFI, provided the microwave power is high
735 enough to approach saturation of the ESR transition for the paramagnetic matrix.¹³⁵⁻¹³⁸
736 Double-resonant structures can be used to concentrate and enhance the microwave and RF
737 magnetic fields at the sample, allowing the use of low-power microwave sources. To
738 further increase the microwave power at the sample, Denysenkov *et al.* use both a
739 resonator and a gyrotron in their high-field DNP spectrometer for liquids.¹³⁹ The increased
740 microwave power provided them a three-fold gain in DNP enhancement. The size of
741 resonant structures for microwaves is inherently restricted due to their smaller
742 wavelengths (< 1 cm at frequencies > 35 GHz), which in turn restricts sample size. To
743 allow larger samples, Dubroca *et al.* have implemented a quasi-optical system that directs
744 gyrotron-sourced high-power microwaves directly to the sample contained in a non-
745 resonant structure.¹⁴⁰

746 **Section IV: Instrumental challenges and outlook for liquid-state DNP NMR.**

747 In this section, we speculate on future directions of method development for liquid-state DNP
748 NMR. Since modern NMR is predominantly conducted at high fields to achieve better resolution
749 and sensitivity, progress in instrumentation development for DNP NMR has also focused on

750 enabling high-field operation in both *ex situ* and *in situ* methodologies. As mentioned previously,
 751 rather large DNP enhancements can be achieved at high fields if the EPR transition can be fully
 752 saturated. Therefore, it is desirable to enhance microwave intensity at the sample volume. *In situ*
 753 and *ex situ* techniques have separate and characteristic challenges. We will discuss sample
 754 containment and flow setups in applications requiring larger or smaller volumes than those
 755 presently available in DNP NMR probes, development of PA, improvements in hardware, and the
 756 development of lab-on-a-chip DNP NMR setups for volume-limited samples. Finally, we mention
 757 advances in the field of low-field DNP NMR, which may be particularly impactful for field
 758 applications and *in vivo* imaging.



759
 760 **Figure 5:** Overview of future directions of research in liquid-state DNP NMR. The figure provides
 761 a simple schematic of the liquid-state DNP NMR setup, with possible areas of development for
 762 various components of the setup.

763 **Challenges for *in situ* DNP NMR at high fields:** *In situ* DNP NMR, particularly when DNP
764 and NMR are conducted under identical physical conditions (field and temperature) is
765 advantageous because it eliminates the problem of loss of polarization during the time taken
766 to go from hyperpolarization conditions to NMR-spectroscopy conditions. However, the only
767 mechanistic pathway for direct liquid-state DNP NMR is through the Overhauser effect, which
768 becomes less efficient at higher fields, because the frequencies corresponding to the ZQ and
769 DQ transitions become much greater than the modulation frequency of the HFI (provided by
770 molecular motions). From a practical standpoint, *in situ* Overhauser DNP with direct NMR
771 detection at the same field is also hindered by the high temperatures required to achieve the
772 necessary correlation times for Overhauser enhancement. (As explained in Section III, point
773 1.2, supercritical DNP is a promising avenue for solving this problem in the case of small-
774 molecule analytes.) Absorption of microwaves by polar solvents such as water can cause
775 further heating, especially at higher frequencies. Lastly, Overhauser enhancement factors can
776 be low for larger molecules due to their longer correlation times. Nonetheless, several recent
777 reports demonstrate that it is possible to achieve enhancements in the range of 10 to 10⁴ in
778 liquid-state *in situ* DNP NMR at high frequencies. In these demonstrations, the high microwave
779 power required to achieve near-saturation conditions is either generated directly by a gyrotron
780 source,^{135,122,124,140} or enhanced at the sample volume using microwave resonant structures
781 (combined with RF resonant structures).¹³⁸

782 **Optimizing sample volume (resonant vs. non-resonant structures for microwave**
783 **excitation):** To achieve appreciable DNP enhancements in liquids, high microwave power is
784 critical in order to saturate the EPR transition. Typically, resonant or non-resonant metallic
785 structures, including coils, cylinders, and cylindrical/rectangular cavities, are used to couple

786 the input microwaves or radiowaves to the sample. Resonators can be used to amplify
787 microwave intensity at the sample when the use of high-power sources such as gyrotrons is
788 expensive or inconvenient. For example, the Prisner group has reported cylinders made of flat
789 metal helices, which are resonant for both EPR (up to 260 GHz) and NMR frequencies.^{135,136,139}
790 The Bennati group use cylindrical TE₀₁₁ cavities to obtain EPR saturation at 94 GHz, while
791 electron nuclear double resonance (ENDOR) coils are used to localize radiowaves over the
792 sample volume.^{137,138} However, the dimensions of resonators become smaller as frequency
793 increases (wavelength decreases), resulting in limits on the sample volume (< 1 μ L). This
794 problem is exacerbated in double-resonant structures, where the wavelength mismatch of
795 microwaves and radiowaves leads to a situation where only a small fraction of the available
796 sample volume in the RF resonator can be filled because the upper limit of sample volume is
797 determined by the microwave resonator. A solution to this problem is to miniaturize the RF
798 resonator so its size is comparable to the EPR resonator.¹⁴¹ However, this still results in sub-
799 microliter sample volumes. Additionally, due to their higher Q -factors, microwave resonant
800 structures have inherently low bandwidths, which deteriorates the sensitivity by allowing DNP
801 enhancement from only a small fraction of the available EPR spectrum. Thus, the use of
802 resonators proves advantageous for mass-limited samples but is less so when the sample
803 quantity is not a limiting factor. Non-resonant structures may be used to localize incident
804 microwaves at the sample volume. These are not size-restricted and can therefore
805 accommodate larger sample volumes. However, these necessitate the use of high-power
806 microwave sources to saturate the EPR transition. Ultimately, structures for localizing
807 microwaves and radiowaves must be chosen to maximize SNR by optimizing sample volume,
808 B_1 intensity, and fraction of the EPR spectrum excited. Additionally, resonators must be

809 designed to separate the regions of electric and magnetic field so that sample heating of high-
810 loss dielectric samples, such as aqueous solutions, is minimized.

811 Large-volume structures are desirable when sample quantity is not limited, so that a large amount
812 of sample may be used to achieve the best possible SNR. On the other hand, many samples are
813 inherently mass-limited as well as concentration-limited, e.g., membrane proteins and other
814 biomacromolecular samples prone to aggregation. Liquid-state DNP NMR of such samples can
815 potentially provide information about dynamics of structure, conformation, and solvation, which
816 is not obtainable through solid-state MAS DNP NMR for all protein samples. Resonators are more
817 suited to such mass-limited and concentration-limited samples. To maximize the SNR in this case,
818 the sample volume should be comparable to the volume of the resonator. Novel approaches are
819 being applied to solve the above-mentioned challenges in resonator design. In Fabry-Perot
820 resonators, the resonator dimension must be limited in only one direction. This allows the sample
821 volume to be extended in the remaining two directions, resulting in large-volume planar structures
822 with sample volumes of tens of microliters.¹⁴²⁻¹⁴⁴ The Smirnov group has developed double-
823 resonant structures in which photonic bandgap microwave resonators are incorporated with NMR
824 coils. These structures are also size-limited in only one dimension, resulting in sample volumes of
825 several microliters.¹⁴⁵

826 ***Ex situ* DNP NMR at high fields:** It is generally accepted that in the case of d-DNP, increasing
827 the field at which DNP is conducted increases the maximum enhancement but also increases the
828 time required to reach this maximum. Further, no appreciable sensitivity gains are obtained after
829 a field of about 7 T. Therefore, further improvements to *ex situ* DNP NMR are likely to focus on
830 first, decreasing loss of polarization between the DNP and NMR steps and second, increasing the
831 amount of hyperpolarized material to offset the expense of time and cryogen while building up

832 hyperpolarization (the second point is particularly important for clinical applications, in which the
833 amount of sample is not a limiting factor).

834 • **High throughput:** Increasing the throughput of the hyperpolarization stage is desirable
835 because: first, it overcomes the time lost during buildup of hyperpolarization, which is a
836 limiting step in d-DNP; and second, it partially overcomes the lack of sample recyclability.
837 Ardenkjær-Larsen *et al.* have reported a d-DNP polarizer that can simultaneously produce
838 up to three hyperpolarized samples of up to 2 g with a buildup time of 20 min.¹⁴⁶ Further,
839 their system uses a closed loop to recycle the cryogen required to cool the sample down for
840 hyperpolarization, easing the massive cryogen requirements of d-DNP. Another similar
841 design of d-DNP spectrometer reported recently can accommodate two samples, and can
842 be modified to accommodate up to four samples.¹⁴⁷ Bornet *et al.* have shown that cross-
843 polarization from ^1H to ^{13}C during the hyperpolarization step can be preserved through
844 dissolution, dramatically increasing the DNP throughput for low-gamma nuclei.¹⁴⁸

845 • **Preserving hyperpolarization:** Developing hardware for efficient transport of
846 hyperpolarized sample is an active area in DNP research, since *ex situ* schemes such as d-
847 DNP are still limited by the problems of sample depolarization during transport and sample
848 dilution in the dissolution step. Kouřil *et al.* have reported a new transportation protocol in
849 which the sample is hyperpolarized and transferred to the site of NMR in the solid form
850 (“bullet DNP”) in 70 ms.¹¹⁵ Dissolution is carried out just before NMR, and the amount of
851 solvent can be adjusted as required for NMR spectroscopy. This makes the method scalable
852 to small volumes.

853 **Polarizing agents:** Exogenous radicals such as TOTAPOL,¹⁴⁹ AMUPOL,¹⁵⁰ BDPA and its
854 derivatives, and trityl are typically used as PAs in DNP NMR. Recent years have seen the

855 development of biradicals, which contain two rigidly linked paramagnetic moieties, that provide
856 improved DNP enhancements, particularly via the cross effect.^{151,152} For applicability at high
857 fields, Lund *et al.* have recently developed ‘TinyPols’, which are water-soluble biradicals with
858 strong dipolar coupling between the two unpaired electrons.¹⁵³ In d-DNP, Gd³⁺-doping has been
859 shown to have a strong influence on polarization enhancement of ¹³C compounds such as
860 pyruvate.¹⁵⁴⁻¹⁵⁶ Below we summarize the most recent developments in PAs, based on different
861 methodologies of solution DNP NMR.

862 • **PA for scalar Overhauser effect:** Earlier reports of direct Overhauser enhancement
863 involved predominantly dipolar HFI of protons, resulting in the conventional thought that
864 enhancements become small as field is increased. While this may be true for
865 hyperpolarization of high- γ nuclei such as protons, the Bennati group has recently shown
866 that enhancement factors of the order of 1000 can be obtained for ¹³C in Overhauser DNP
867 for fields in the range of 1 T to 10 T.¹³⁸ These enhancements have been explained as arising
868 from the scalar HFI between the ¹³C-containing molecule and paramagnetic radical, and
869 the key features of the mechanism have been identified.¹⁵⁷ Further elucidation of the
870 mechanistic origins of these large ¹³C enhancements is likely to result in new PA for direct
871 Overhauser enhancement in the solution state.^{158,159}

872 • **PA for *ex situ* techniques:** In *ex situ* techniques where hyperpolarization and NMR/MRI
873 are separated by a transport step, the paramagnetic matrix is required for DNP but becomes
874 undesirable in the transport and NMR steps because it causes loss of polarization and
875 broadening of NMR lines. The PA may be separated from the sample by physical methods,
876 e.g., filterable agents^{160,161} or immobilization on a solid substrate.^{162,120,121,163} An elegant
877 means to generate longer-lasting, transportable hyperpolarized samples is photo-generation

878 of radicals that re-combine when the temperature is increased after the hyperpolarization
879 step.^{164,165} This provides a way to eliminate the undesirable paramagnetic matrix after the
880 hyperpolarization step.

881 • **Triplet DNP for liquid samples:** Photo-induced triplet states can be used to generate
882 hyperpolarization that is independent of temperature and magnetic field strength.¹⁶⁶
883 Kagawa *et al.* have recently reported protocols for preparing a wide range of
884 hyperpolarized samples at room temperature using the photo-induced triplet state of
885 pentacene,¹⁶⁷ and have further used triplet DNP in conjunction with the d-DNP protocol to
886 obtain hyperpolarized solutions at both low and high fields.^{168,169} The Yanai group is active
887 in developing PAs with favorable properties such as improved air stability¹⁷⁰ and water-
888 solubility.¹⁷¹ The Bennati group has reported liquid-state triplet DNP using photoexcitable
889 fullerene-nitroxide derivatives.¹⁷²

890 **Mass-limited samples:** Some examples of applications for mass-limited and concentration-
891 limited liquid-state samples that particularly benefit from hyperpolarization include: identification
892 of natural products, metabolites of pharmaceuticals and agrochemicals, and characterization of
893 compounds from combinatorial chemistry;^{173,174} studies of structure and dynamics of membrane
894 proteins and other biomacromolecules that are difficult to isolate and prone to aggregation at the
895 high concentration typically needed for standard NMR measurements;¹⁷⁵ and in-cell NMR.^{176,177}
896 Such applications require the ability to sense both small volumes and small concentrations.
897 Double-resonant structures provide sample volumes of nanoliters but the fill factor for the RF part
898 of the double-resonator is very small, resulting in poor sensitivity. (For comparison, CapNMR
899 finds widespread use in solution NMR but requires microliter volumes.¹⁷⁸) Planar microcoils are
900 easier to fabricate down to nL volumes, and find applications in on-chip NMR devices.¹⁷⁹

901 Recently, Solmaz *et al.* have demonstrated a silicon-chip-based device for DNP NMR of aqueous
902 solutions of TEMPO radical at room temperature.¹⁸⁰ A sample volume of about 1 nL is contained
903 in a capillary that is placed over the double NMR/ESR microcoils.

904 **Low-field DNP NMR:** Although recent developments in DNP NMR have focused on extending
905 applicability to high-field NMR, low-field NMR is also an emerging area that stands to benefit
906 from sensitivity enhancements provided by DNP. Developments in low-field DNP NMR seek to
907 increase resolution while maximizing hyperpolarization. Maly *et al.* have shown recently that is
908 possible to improve both sensitivity and resolution even at low fields by improving field
909 homogeneity.¹⁸¹ The ability to conduct DNP NMR at low fields is also desirable for portable
910 setups.⁹⁷

911 **Conclusion:** In this review, we have attempted to provide an overview of the conceptual basis,
912 applications, and instrumentation for a wide range of schemes for liquid-state CW DNP NMR.
913 Liquid-state DNP has broad potential applications, particularly in the areas of metabolite
914 characterization, imaging, characterization of transient species in reaction mechanisms, and studies
915 of structure, conformation, and solvation dynamics for precious biomolecular samples.
916 Approaches to liquid-state DNP NMR must take into account the sample type, size, and
917 application. Some applications involve samples that are inherently limited in quantity and/or
918 concentration (metabolomics, transient species, some biomacromolecular samples). On the other
919 hand, in applications like imaging, it is desirable to have high throughputs of hyperpolarized
920 sample, and amount of sample is not a limiting factor. In *in vivo* imaging, the hyperpolarized
921 sample is injected into a specimen and thus, there is a natural separation of locations for
922 hyperpolarization and NMR. Such applications necessitate the use of *ex situ* DNP methodologies
923 such as dissolution DNP. Direct DNP in liquids is of interest for biomacromolecular systems that

924 are difficult to express, purify, and reconstitute, and that may become denatured and/or aggregate
925 through rapid changes in physical conditions. While brute-force methods may sometimes offer
926 greater effective sensitivity at high fields, DNP promises sensitivity gains at low and intermediate
927 frequencies. In general, all DNP methodologies would benefit from high-field operability to take
928 advantage of the high resolution and sensitivity provided by modern high-field NMR
929 spectrometers. On the other hand, there is interest in improving the resolution of low-field DNP
930 since larger enhancements can be obtained at low fields and, additionally, because low fields are
931 favorable for applications such as *in vivo* imaging and compact spectrometers. PA for which the
932 scalar HFI is dominant are likely to facilitate greater DNP enhancements at high fields. Another
933 way to obtain field-independent DNP enhancement is using photo-excited triplets to saturate the
934 electronic spin system. Supercritical DNP may also be impactful for high-field NMR of small-
935 molecule analytes by faster relaxation frequencies, and by providing a proton-free solvent that is
936 not prone to dielectric heating. Most detection schemes for DNP NMR employ high-power
937 microwave sources such as gyrotrons to saturate the EPR transition. On the other hand, double-
938 resonant structures eliminate the need for using high-power microwave sources but require
939 advances in miniaturization to confine radiowaves and microwaves in similar volumes. The varied
940 methodologies of *ex situ* and *in situ* liquid DNP provide a large playing field with multi-faceted
941 opportunities for advancement, with the ultimate promise of revealing hitherto unavailable
942 information about dynamic processes occurring in liquids.

943

944 **Acknowledgments**

945 Nandita Abhyankar acknowledges partial support under the Cooperative Research Agreement
946 between the University of Maryland and the National Institute of Standards and Technology

947 Physical Measurement Laboratory, Award 70NANB14H209, through the University of
948 Maryland, and through NIGMS Award # R21GM134406.

949 **References:**

- 950 (1) Barnes, A. B.; De Paëpe, G.; van der Wel, P. C. A.; Hu, K.-N.; Joo, C.-G.; Bajaj, V. S.;
951 Mak-Jurkauskas, M. L.; Sirigiri, J. R.; Herzfeld, J.; Temkin, R. J.; Griffin, R. G. High-Field
952 Dynamic Nuclear Polarization for Solid and Solution Biological NMR. *Appl. Magn. Reson.*
953 **2008**, *34* (3–4), 237–263. <https://doi.org/10.1007/s00723-008-0129-1>.
- 954 (2) Lacabanne, D.; Fogeron, M.-L.; Wiegand, T.; Cadalbert, R.; Meier, B. H.; Böckmann, A.
955 Protein Sample Preparation for Solid-State NMR Investigations. *Prog. Nucl. Magn. Reson.*
956 *Spectrosc.* **2019**, *110*, 20–33. <https://doi.org/10.1016/j.pnmrs.2019.01.001>.
- 957 (3) Maly, T.; Debelouchina, G. T.; Bajaj, V. S.; Hu, K.-N.; Joo, C.-G.; Mak-Jurkauskas, M. L.;
958 Sirigiri, J. R.; van der Wel, P. C. A.; Herzfeld, J.; Temkin, R. J.; Griffin, R. G. Dynamic
959 Nuclear Polarization at High Magnetic Fields. *J. Chem. Phys.* **2008**, *128* (5), 052211.
960 <https://doi.org/10.1063/1.2833582>.
- 961 (4) Corzilius, B. High-Field Dynamic Nuclear Polarization. *Annu. Rev. Phys. Chem.* **2020**, *71*
962 (1), 143–170. <https://doi.org/10.1146/annurev-physchem-071119-040222>.
- 963 (5) Can, T. V.; Ni, Q. Z.; Griffin, R. G. Mechanisms of Dynamic Nuclear Polarization in
964 Insulating Solids. *Spec. Issue Recent Achiev. New Dir. Biomol. Solid State NMR* **2015**, *253*,
965 23–35. <https://doi.org/10.1016/j.jmr.2015.02.005>.
- 966 (6) Bennati, M.; Tkach, I.; Türke, M.-T. Dynamic Nuclear Polarization in Liquids. In *Electron*
967 *Paramagnetic Resonance*; Gilbert, B. C., Murphy, D. M., Chechik, V., Eds.; Royal Society
968 of Chemistry: Cambridge, 2010; Vol. 22, pp 155–182.
969 <https://doi.org/10.1039/9781849730877-00155>.
- 970 (7) Ravera, E.; Luchinat, C.; Parigi, G. Basic Facts and Perspectives of Overhauser DNP NMR.
971 *J. Magn. Reson.* **2016**, *264*, 78–87. <https://doi.org/10.1016/j.jmr.2015.12.013>.
- 972 (8) van Bentum, J.; van Meerten, B.; Sharma, M.; Kentgens, A. Perspectives on DNP-
973 Enhanced NMR Spectroscopy in Solutions. *J. Magn. Reson.* **2016**, *264*, 59–67.
974 <https://doi.org/10.1016/j.jmr.2016.01.010>.
- 975 (9) Hausser, K. H.; Stehlik, D. Dynamic Nuclear Polarization in Liquids. In *Advances in*
976 *Magnetic and Optical Resonance*; Elsevier, 1968; Vol. 3, pp 79–139.
977 <https://doi.org/10.1016/B978-1-4832-3116-7.50010-2>.
- 978 (10) Overhauser, A. W. Polarization of Nuclei in Metals. *Phys. Rev.* **1953**, *92* (2), 411–415.
979 <https://doi.org/10.1103/PhysRev.92.411>.
- 980 (11) Abragam, A.; Goldman, M. Principles of Dynamic Nuclear Polarisation. *Rep. Prog. Phys.*
981 **1978**, *41* (3), 395–467. <https://doi.org/10.1088/0034-4885/41/3/002>.
- 982 (12) Carver, T. R.; Slichter, C. P. Polarization of Nuclear Spins in Metals. *Phys. Rev.* **1953**, *92*
983 (1), 212–213. <https://doi.org/10.1103/PhysRev.92.212.2>.
- 984 (13) Abragam, A. Overhauser Effect in Nonmetals. *Phys. Rev.* **1955**, *98* (6), 1729–1735.
985 <https://doi.org/10.1103/PhysRev.98.1729>.
- 986 (14) Solomon, I. Relaxation Processes in a System of Two Spins. *Phys. Rev.* **1955**, *99* (2), 559–
987 565. <https://doi.org/10.1103/PhysRev.99.559>.

- 988 (15) Ardenkjaer-Larsen, J. H.; Fridlund, B.; Gram, A.; Hansson, G.; Hansson, L.; Lerche, M. H.;
989 Servin, R.; Thaning, M.; Golman, K. Increase in Signal-to-Noise Ratio of > 10,000 Times
990 in Liquid-State NMR. *Proc. Natl. Acad. Sci.* **2003**, *100* (18), 10158–10163.
991 <https://doi.org/10.1073/pnas.1733835100>.
- 992 (16) Wang, X.; Isley III, W. C.; Salido, S. I.; Sun, Z.; Song, L.; Tsai, K. H.; Cramer, C. J.; Dorn,
993 H. C. Optimization and Prediction of the Electron–Nuclear Dipolar and Scalar Interaction
994 in ^1H and ^{13}C Liquid State Dynamic Nuclear Polarization. *Chem. Sci.* **2015**, *6* (11), 6482–
995 6495. <https://doi.org/10.1039/C5SC02499D>.
- 996 (17) Gizatullin, B.; Gafurov, M.; Vakhin, A.; Rodionov, A.; Mamin, G.; Orlinskii, S.; Mattea,
997 C.; Stapf, S. Native Vanadyl Complexes in Crude Oil as Polarizing Agents for *In Situ*
998 Proton Dynamic Nuclear Polarization. *Energy Fuels* **2019**, *33* (11), 10923–10932.
999 <https://doi.org/10.1021/acs.energyfuels.9b03049>.
- 1000 (18) Hwang, C. F.; Hill, D. A. New Effect in Dynamic Polarization. *Phys. Rev. Lett.* **1967**, *18*
1001 (4), 110–112. <https://doi.org/10.1103/PhysRevLett.18.110>.
- 1002 (19) Hwang, C. F.; Hill, D. A. Phenomenological Model for the New Effect in Dynamic
1003 Polarization. *Phys. Rev. Lett.* **1967**, *19* (18), 1011–1014.
1004 <https://doi.org/10.1103/PhysRevLett.19.1011>.
- 1005 (20) Borghini, M. Spin-Temperature Model of Nuclear Dynamic Polarization Using Free
1006 Radicals. *Phys. Rev. Lett.* **1968**, *20* (9), 419–421.
1007 <https://doi.org/10.1103/PhysRevLett.20.419>.
- 1008 (21) Wenckebach, W. Th. Dynamic Nuclear Polarization via Thermal Mixing: Beyond the High
1009 Temperature Approximation. *J. Magn. Reson.* **2017**, *277*, 68–78.
1010 <https://doi.org/10.1016/j.jmr.2017.01.020>.
- 1011 (22) Equbal, A.; Leavesley, A.; Jain, S. K.; Han, S. Cross-Effect Dynamic Nuclear Polarization
1012 Explained: Polarization, Depolarization, and Oversaturation. *J. Phys. Chem. Lett.* **2019**, *10*
1013 (3), 548–558. <https://doi.org/10.1021/acs.jpcclett.8b02834>.
- 1014 (23) Grazia Concilio, M.; Soundararajan, M.; Frydman, L.; Kuprov, I. High-Field Solution State
1015 DNP Using Cross-Correlations. *J. Magn. Reson.* **2021**, 106940.
1016 <https://doi.org/10.1016/j.jmr.2021.106940>.
- 1017 (24) Kundu, K.; Feintuch, A.; Vega, S. Theoretical Aspects of the Cross Effect Enhancement of
1018 Nuclear Polarization under Static Dynamic Nuclear Polarization Conditions. *J. Phys. Chem.*
1019 *Lett.* **2019**, *10* (8), 1769–1778. <https://doi.org/10.1021/acs.jpcclett.8b03615>.
- 1020 (25) Equbal, A.; Li, Y.; Tabassum, T.; Han, S. Crossover from a Solid Effect to Thermal Mixing
1021 ^1H Dynamic Nuclear Polarization with Trityl-OX063. *J. Phys. Chem. Lett.* **2020**, *11* (9),
1022 3718–3723. <https://doi.org/10.1021/acs.jpcclett.0c00830>.
- 1023 (26) Wangsness, R. K.; Bloch, F. The Dynamical Theory of Nuclear Induction. *Phys. Rev.* **1953**,
1024 *89* (4), 728–739. <https://doi.org/10.1103/PhysRev.89.728>.
- 1025 (27) Redfield, A. G. On the Theory of Relaxation Processes. *IBM J. Res. Dev.* **1957**, *1* (1), 19–
1026 31. <https://doi.org/10.1147/rd.11.0019>.
- 1027 (28) Karabanov, A.; Kwiatkowski, G.; Perotto, C. U.; Wiśniewski, D.; McMaster, J.;
1028 Lesanovsky, I.; Köckenberger, W. Dynamic Nuclear Polarisation by Thermal Mixing:
1029 Quantum Theory and Macroscopic Simulations. *Phys. Chem. Chem. Phys.* **2016**, *18* (43),
1030 30093–30104. <https://doi.org/10.1039/C6CP04345C>.
- 1031 (29) Kundu, K.; Feintuch, A.; Vega, S. Theoretical Aspects of the Cross Effect Enhancement of
1032 Nuclear Polarization under Static Dynamic Nuclear Polarization Conditions. *J. Phys. Chem.*
1033 *Lett.* **2019**, *10* (8), 1769–1778. <https://doi.org/10.1021/acs.jpcclett.8b03615>.

- 1034 (30) Equbal, A.; Li, Y.; Tabassum, T.; Han, S. Crossover from a Solid Effect to Thermal Mixing
1035 ¹H Dynamic Nuclear Polarization with Trityl-OX063. *J. Phys. Chem. Lett.* **2020**, *11* (9),
1036 3718–3723. <https://doi.org/10.1021/acs.jpcclett.0c00830>.
- 1037 (31) Corzilius, B. Theory of Solid Effect and Cross Effect Dynamic Nuclear Polarization with
1038 Half-Integer High-Spin Metal Polarizing Agents in Rotating Solids. *Phys. Chem. Chem.*
1039 *Phys.* **2016**, *18* (39), 27190–27204. <https://doi.org/10.1039/C6CP04621E>.
- 1040 (32) Lumata, L.; Jindal, A. K.; Merritt, M. E.; Malloy, C. R.; Sherry, A. D.; Kovacs, Z. DNP by
1041 Thermal Mixing under Optimized Conditions Yields > 60 000-Fold Enhancement of ⁸⁹Y
1042 NMR Signal. *J. Am. Chem. Soc.* **2011**, *133* (22), 8673–8680.
1043 <https://doi.org/10.1021/ja201880y>.
- 1044 (33) Giraudeau, P. Challenges and Perspectives in Quantitative NMR: Challenges and
1045 Perspectives in Quantitative NMR. *Magn. Reson. Chem.* **2017**, *55* (1), 61–69.
1046 <https://doi.org/10.1002/mrc.4475>.
- 1047 (34) Franck, J. M.; Han, S. Overhauser Dynamic Nuclear Polarization for the Study of
1048 Hydration Dynamics, Explained. In *Methods in Enzymology*; Elsevier, 2019; Vol. 615, pp
1049 131–175. <https://doi.org/10.1016/bs.mie.2018.09.024>.
- 1050 (35) Armstrong, B. D.; Choi, J.; López, C.; Wesener, D. A.; Hubbell, W.; Cavagnero, S.; Han, S.
1051 Site-Specific Hydration Dynamics in the Nonpolar Core of a Molten Globule by Dynamic
1052 Nuclear Polarization of Water. *J. Am. Chem. Soc.* **2011**, *133* (15), 5987–5995.
1053 <https://doi.org/10.1021/ja111515s>.
- 1054 (36) McCarney, E. R.; Armstrong, B. D.; Kausik, R.; Han, S. Dynamic Nuclear Polarization
1055 Enhanced Nuclear Magnetic Resonance and Electron Spin Resonance Studies of Hydration
1056 and Local Water Dynamics in Micelle and Vesicle Assemblies. *Langmuir* **2008**, *24* (18),
1057 10062–10072. <https://doi.org/10.1021/la800334k>.
- 1058 (37) Armstrong, B. D.; Han, S. Overhauser Dynamic Nuclear Polarization to Study Local Water
1059 Dynamics. *J. Am. Chem. Soc.* **2009**, *131* (13), 4641–4647.
1060 <https://doi.org/10.1021/ja809259q>.
- 1061 (38) Segawa, T. F.; Doppelbauer, M.; Garbuio, L.; Doll, A.; Polyhach, Y. O.; Jeschke, G. Water
1062 Accessibility in a Membrane-Inserting Peptide Comparing Overhauser DNP and Pulse EPR
1063 Methods. *J. Chem. Phys.* **2016**, *144* (19), 194201. <https://doi.org/10.1063/1.4948988>.
- 1064 (39) Chaubey, B.; Dey, A.; Banerjee, A.; Chandrakumar, N.; Pal, S. Assessment of the Role of
1065 2,2,2-Trifluoroethanol Solvent Dynamics in Inducing Conformational Transitions in
1066 Melittin: An Approach with Solvent ¹⁹F Low-Field NMR Relaxation and Overhauser
1067 Dynamic Nuclear Polarization Studies. *J. Phys. Chem. B* **2020**, *124* (28), 5993–6003.
1068 <https://doi.org/10.1021/acs.jpcc.0c03544>.
- 1069 (40) Kim, J.; Liu, M.; Hilty, C. Modeling of Polarization Transfer Kinetics in Protein Hydration
1070 Using Hyperpolarized Water. *J. Phys. Chem. B* **2017**, *121* (27), 6492–6498.
1071 <https://doi.org/10.1021/acs.jpcc.7b03052>.
- 1072 (41) Kadeřávek, P.; Ferrage, F.; Bodenhausen, G.; Kurzbach, D. High-Resolution NMR of
1073 Folded Proteins in Hyperpolarized Physiological Solvents. *Chem. - Eur. J.* **2018**, *24* (51),
1074 13418–13423. <https://doi.org/10.1002/chem.201802885>.
- 1075 (42) Chappuis, Q.; Milani, J.; Vuichoud, B.; Bornet, A.; Gossert, A. D.; Bodenhausen, G.;
1076 Jannin, S. Hyperpolarized Water to Study Protein–Ligand Interactions. *J. Phys. Chem. Lett.*
1077 **2015**, *6* (9), 1674–1678. <https://doi.org/10.1021/acs.jpcclett.5b00403>.

- 1078 (43) Kim, J.; Mandal, R.; Hilty, C. Observation of Fast Two-Dimensional NMR Spectra during
1079 Protein Folding Using Polarization Transfer from Hyperpolarized Water. *J. Phys. Chem.*
1080 *Lett.* **2019**, *10* (18), 5463–5467. <https://doi.org/10.1021/acs.jpcclett.9b02197>.
- 1081 (44) Akbey, Ü.; Oschkinat, H. Structural Biology Applications of Solid State MAS DNP NMR.
1082 *J. Magn. Reson.* **2016**, *269*, 213–224. <https://doi.org/10.1016/j.jmr.2016.04.003>.
- 1083 (45) Jaudzems, K.; Polenova, T.; Pintacuda, G.; Oschkinat, H.; Lesage, A. DNP NMR of
1084 Biomolecular Assemblies. *J. Struct. Biol.* **2019**, *206* (1), 90–98.
1085 <https://doi.org/10.1016/j.jsb.2018.09.011>.
- 1086 (46) Kim, J.; Mandal, R.; Hilty, C. Characterization of Membrane Protein-Lipid Interactions in
1087 Unfolded OmpX with Enhanced Time Resolution by Hyperpolarized NMR. *ChemBioChem*
1088 **2020**, *cbic.202000271*. <https://doi.org/10.1002/cbic.202000271>.
- 1089 (47) Szekely, O.; Olsen, G. L.; Felli, I. C.; Frydman, L. High-Resolution 2D NMR of Disordered
1090 Proteins Enhanced by Hyperpolarized Water. *Anal. Chem.* **2018**, *90* (10), 6169–6177.
1091 <https://doi.org/10.1021/acs.analchem.8b00585>.
- 1092 (48) Wang, Y.; Kim, J.; Hilty, C. Determination of Protein–Ligand Binding Modes Using Fast
1093 Multi-Dimensional NMR with Hyperpolarization. *Chem. Sci.* **2020**, *11* (23), 5935–5943.
1094 <https://doi.org/10.1039/D0SC00266F>.
- 1095 (49) Wang, Y.; Ragavan, M.; Hilty, C. Site Specific Polarization Transfer from a
1096 Hyperpolarized Ligand of Dihydrofolate Reductase. *J. Biomol. NMR* **2016**, *65* (1), 41–48.
1097 <https://doi.org/10.1007/s10858-016-0037-x>.
- 1098 (50) Lee, Y.; Zeng, H.; Mazur, A.; Wegstroth, M.; Carlomagno, T.; Reese, M.; Lee, D.; Becker,
1099 S.; Griesinger, C.; Hilty, C. Hyperpolarized Binding Pocket Nuclear Overhauser Effect for
1100 Determination of Competitive Ligand Binding. *Angew. Chem. Int. Ed.* **2012**, *51* (21), 5179–
1101 5182. <https://doi.org/10.1002/anie.201201003>.
- 1102 (51) Min, H.; Sekar, G.; Hilty, C. Polarization Transfer from Ligands Hyperpolarized by
1103 Dissolution Dynamic Nuclear Polarization for Screening in Drug Discovery.
1104 *ChemMedChem* **2015**, *10* (9), 1559–1563. <https://doi.org/10.1002/cmdc.201500241>.
- 1105 (52) Brogi, S.; Ramalho, T. C.; Kuca, K.; Medina-Franco, J. L.; Valko, M. Editorial: *In Silico*
1106 Methods for Drug Design and Discovery. *Front. Chem.* **2020**, *8*, 612.
1107 <https://doi.org/10.3389/fchem.2020.00612>.
- 1108 (53) Bowen, S.; Hilty, C. Time-Resolved Dynamic Nuclear Polarization Enhanced NMR
1109 Spectroscopy. *Angew. Chem. Int. Ed.* **2008**, *47* (28), 5235–5237.
1110 <https://doi.org/10.1002/anie.200801492>.
- 1111 (54) Bowen, S.; Hilty, C. Temporal Chemical Shift Correlations in Reactions Studied by
1112 Hyperpolarized Nuclear Magnetic Resonance. *Anal. Chem.* **2009**, *81* (11), 4543–4547.
1113 <https://doi.org/10.1021/ac900456q>.
- 1114 (55) Zhang, G.; Schilling, F.; Glaser, S. J.; Hilty, C. Reaction Monitoring Using Hyperpolarized
1115 NMR with Scaling of Heteronuclear Couplings by Optimal Tracking. *J. Magn. Reson.*
1116 **2016**, *272*, 123–128. <https://doi.org/10.1016/j.jmr.2016.09.006>.
- 1117 (56) Jensen, P. R.; Meier, S. Catalytic Cycle of Carbohydrate Dehydration by Lewis Acids:
1118 Structures and Rates from Synergism of Conventional and DNP NMR. *Chem. Commun.*
1119 **2020**, *56* (46), 6245–6248. <https://doi.org/10.1039/D0CC01756F>.
- 1120 (57) Jensen, P. R.; Meier, S.; Ardenkjær-Larsen, J. H.; Duus, J. Ø.; Karlsson, M.; Lerche, M. H.
1121 Detection of Low-Populated Reaction Intermediates with Hyperpolarized NMR. *Chem.*
1122 *Commun.* **2009**, No. 34, 5168. <https://doi.org/10.1039/b910626j>.

- 1123 (58) Boeg, P. A.; Duus, J. Ø.; Ardenkjær-Larsen, J. H.; Karlsson, M.; Mossin, S. Real-Time
1124 Detection of Intermediates in Rhodium-Catalyzed Hydrogenation of Alkynes and Alkenes
1125 by Dissolution DNP. *J. Phys. Chem. C* **2019**, *123* (15), 9949–9956.
1126 <https://doi.org/10.1021/acs.jpcc.9b01376>.
- 1127 (59) Chen, C.-H.; Shih, W.-C.; Hilty, C. *In Situ* Determination of Tacticity, Deactivation, and
1128 Kinetics in [*Rac*-(C₂H₄(1-Indenyl)₂)ZrMe][B(C₆F₅)₄] and [Cp₂ZrMe][B(C₆F₅)₄]-Catalyzed
1129 Polymerization of 1-Hexene Using ¹³C Hyperpolarized NMR. *J. Am. Chem. Soc.* **2015**, *137*
1130 (21), 6965–6971. <https://doi.org/10.1021/jacs.5b04479>.
- 1131 (60) Lee, Y.; Heo, G. S.; Zeng, H.; Wooley, K. L.; Hilty, C. Detection of Living Anionic
1132 Species in Polymerization Reactions Using Hyperpolarized NMR. *J. Am. Chem. Soc.* **2013**,
1133 *135* (12), 4636–4639. <https://doi.org/10.1021/ja4001008>.
- 1134 (61) Weber, E. M. M.; Kress, T.; Abergel, D.; Sewsum, S.; Azaïs, T.; Kurzbach, D. Assessing
1135 the Onset of Calcium Phosphate Nucleation by Hyperpolarized Real-Time NMR. *Anal.*
1136 *Chem.* **2020**, *92* (11), 7666–7673. <https://doi.org/10.1021/acs.analchem.0c00516>.
- 1137 (62) Lerche, M. H.; Meier, S.; Jensen, P. R.; Baumann, H.; Petersen, B. O.; Karlsson, M.; Duus,
1138 J. Ø.; Ardenkjær-Larsen, J. H. Study of Molecular Interactions with ¹³C DNP-NMR. *J.*
1139 *Magn. Reson.* **2010**, *203* (1), 52–56. <https://doi.org/10.1016/j.jmr.2009.11.020>.
- 1140 (63) Liu, M.; Zhang, G.; Mahanta, N.; Lee, Y.; Hilty, C. Measurement of Kinetics and Active
1141 Site Distances in Metalloenzymes Using Paramagnetic NMR with ¹³C Hyperpolarization. *J.*
1142 *Phys. Chem. Lett.* **2018**, *9* (9), 2218–2221. <https://doi.org/10.1021/acs.jpcllett.8b00350>.
- 1143 (64) Shishmarev, D.; Wright, A. J.; Rodrigues, T. B.; Pileio, G.; Stevanato, G.; Brindle, K. M.;
1144 Kuchel, P. W. Sub-Minute Kinetics of Human Red Cell Fumarase: ¹H Spin-Echo NMR
1145 Spectroscopy and ¹³C Rapid-Dissolution Dynamic Nuclear Polarization. *NMR Biomed.*
1146 **2018**, *31* (3), e3870. <https://doi.org/10.1002/nbm.3870>.
- 1147 (65) Drachman, N.; Kadlecek, S.; Duncan, I.; Rizi, R. Quantifying Reaction Kinetics of the
1148 Non-Enzymatic Decarboxylation of Pyruvate and Production of Peroxymonocarbonate with
1149 Hyperpolarized ¹³C-NMR. *Phys. Chem. Chem. Phys.* **2017**, *19* (29), 19316–19325.
1150 <https://doi.org/10.1039/C7CP02041D>.
- 1151 (66) Timm, K. N.; Hu, D.-E.; Williams, M.; Wright, A. J.; Kettunen, M. I.; Kennedy, B. W. C.;
1152 Larkin, T. J.; Dzien, P.; Marco-Rius, I.; Bohndiek, S. E.; Brindle, K. M. Assessing
1153 Oxidative Stress in Tumors by Measuring the Rate of Hyperpolarized [1- ¹³C]-
1154 Dehydroascorbic Acid Reduction Using ¹³C Magnetic Resonance Spectroscopy. *J. Biol.*
1155 *Chem.* **2017**, *292* (5), 1737–1748. <https://doi.org/10.1074/jbc.M116.761536>.
- 1156 (67) Tickner, Ben. J.; Rayner, P. J.; Duckett, S. B. Using SABRE Hyperpolarized ¹³C NMR
1157 Spectroscopy to Interrogate Organic Transformations of Pyruvate. *Anal. Chem.* **2020**, *92*
1158 (13), 9095–9103. <https://doi.org/10.1021/acs.analchem.0c01334>.
- 1159 (68) Bowen, S.; Sekar, G.; Hilty, C. Rapid Determination of Biosynthetic Pathways Using
1160 Fractional Isotope Enrichment and High-Resolution Dynamic Nuclear Polarization
1161 Enhanced NMR: BIOSYNTHETIC PATHWAYS STUDIED BY HYPERRPOLARIZED
1162 NMR. *NMR Biomed.* **2011**, *24* (8), 1016–1022. <https://doi.org/10.1002/nbm.1679>.
- 1163 (69) Kjeldsen, C.; Ardenkjær-Larsen, J. H.; Duus, Jens. Ø. Unexpected Anomeric Acceptor
1164 Preference Observed Using DDNP NMR for Transglycosylation Studies of β-
1165 Galactosidases. *Biochemistry* **2020**, *59* (31), 2903–2908.
1166 <https://doi.org/10.1021/acs.biochem.0c00390>.
- 1167 (70) Golman, K.; in 't Zandt, R.; Thaning, M. Real-Time Metabolic Imaging. *Proc. Natl. Acad.*
1168 *Sci.* **2006**, *103* (30), 11270–11275. <https://doi.org/10.1073/pnas.0601319103>.

- 1169 (71) Lerche, M. H.; Meier, S.; Jensen, P. R.; Hustvedt, S.-O.; Karlsson, M.; Duus, J. Ø.;
1170 Ardenkjaer-Larsen, J. H. Quantitative Dynamic Nuclear Polarization-NMR on Blood
1171 Plasma for Assays of Drug Metabolism. *NMR Biomed.* **2011**, *24* (1), 96–103.
1172 <https://doi.org/10.1002/nbm.1561>.
- 1173 (72) Bohndiek, S. E.; Kettunen, M. I.; Hu, D.; Kennedy, B. W. C.; Boren, J.; Gallagher, F. A.;
1174 Brindle, K. M. Hyperpolarized [1- ¹³C]-Ascorbic and Dehydroascorbic Acid: Vitamin C as
1175 a Probe for Imaging Redox Status *in Vivo*. *J. Am. Chem. Soc.* **2011**, *133* (30), 11795–
1176 11801. <https://doi.org/10.1021/ja2045925>.
- 1177 (73) Simmler, C.; Napolitano, J. G.; McAlpine, J. B.; Chen, S.-N.; Pauli, G. F. Universal
1178 Quantitative NMR Analysis of Complex Natural Samples. *Curr. Opin. Biotechnol.* **2014**,
1179 *25*, 51–59. <https://doi.org/10.1016/j.copbio.2013.08.004>.
- 1180 (74) Dzien, P.; Fages, A.; Jona, G.; Brindle, K. M.; Schwaiger, M.; Frydman, L. Following
1181 Metabolism in Living Microorganisms by Hyperpolarized ¹H NMR. *J. Am. Chem. Soc.*
1182 **2016**, *138* (37), 12278–12286. <https://doi.org/10.1021/jacs.6b07483>.
- 1183 (75) Jensen, P. R.; Karlsson, M.; Lerche, M. H.; Meier, S. Real-Time DNP NMR Observations
1184 of Acetic Acid Uptake, Intracellular Acidification, and of Consequences for Glycolysis and
1185 Alcoholic Fermentation in Yeast. *Chem. - Eur. J.* **2013**, *19* (40), 13288–13293.
1186 <https://doi.org/10.1002/chem.201302429>.
- 1187 (76) Lerche, M. H.; Jensen, P. R.; Karlsson, M.; Meier, S. NMR Insights into the Inner
1188 Workings of Living Cells. *Anal. Chem.* **2015**, *87* (1), 119–132.
1189 <https://doi.org/10.1021/ac501467x>.
- 1190 (77) Kumar, A.; Kuhn, L.; Balbach, J. In-Cell NMR: Analysis of Protein–Small Molecule
1191 Interactions, Metabolic Processes, and Protein Phosphorylation. *Int. J. Mol. Sci.* **2019**, *20*
1192 (2), 378. <https://doi.org/10.3390/ijms20020378>.
- 1193 (78) Warnet, X. L.; Arnold, A. A.; Marcotte, I.; Warschawski, D. E. In-Cell Solid-State NMR:
1194 An Emerging Technique for the Study of Biological Membranes. *Biophys. J.* **2015**, *109*
1195 (12), 2461–2466. <https://doi.org/10.1016/j.bpj.2015.10.041>.
- 1196 (79) Judge, P. T.; Sesti, E. L.; Price, L. E.; Albert, B. J.; Alaniva, N.; Saliba, E. P.; Halbritter, T.;
1197 Sigurdsson, S. Th.; Kyei, G. B.; Barnes, A. B. Dynamic Nuclear Polarization with Electron
1198 Decoupling in Intact Human Cells and Cell Lysates. *J. Phys. Chem. B* **2020**, *124* (12),
1199 2323–2330. <https://doi.org/10.1021/acs.jpcc.9b10494>.
- 1200 (80) Zhelev, Z.; Bakalova, R.; Aoki, I.; Matsumoto, K.; Gadjeva, V.; Anzai, K.; Kanno, I.
1201 Nitroxyl Radicals for Labeling of Conventional Therapeutics and Noninvasive Magnetic
1202 Resonance Imaging of Their Permeability for Blood–Brain Barrier: Relationship between
1203 Structure, Blood Clearance, and MRI Signal Dynamic in the Brain. *Mol. Pharm.* **2009**, *6*
1204 (2), 504–512. <https://doi.org/10.1021/mp800175k>.
- 1205 (81) Zhelev, Z.; Bakalova, R.; Aoki, I.; Matsumoto, K.; Gadjeva, V.; Anzai, K.; Kanno, I.
1206 Nitroxyl Radicals as Low Toxic Spin-Labels for Non-Invasive Magnetic Resonance
1207 Imaging of Blood–Brain Barrier Permeability for Conventional Therapeutics. *Chem*
1208 *Commun* **2009**, No. 1, 53–55. <https://doi.org/10.1039/B816878D>.
- 1209 (82) Kishimoto, S.; Oshima, N.; Krishna, M. C.; Gillies, R. J. Direct and Indirect Assessment of
1210 Cancer Metabolism Explored by MRI. *NMR Biomed.* **2019**, *32* (10).
1211 <https://doi.org/10.1002/nbm.3966>.
- 1212 (83) Asavei, T.; Bobeica, M.; Nastasa, V.; Manda, G.; Naftanaila, F.; Bratu, O.; Mischianu, D.;
1213 Cernaianu, M. O.; Ghenuche, P.; Savu, D.; Stutman, D.; Tanaka, K. A.; Radu, M.; Doria,

- 1214 D.; Vasos, P. R. Laser-driven Radiation: Biomarkers for Molecular Imaging of High Dose-
1215 rate Effects. *Med. Phys.* **2019**, *46* (10). <https://doi.org/10.1002/mp.13741>.
- 1216 (84) Qin, H.; Zhang, V.; Bok, R. A.; Santos, R. D.; Cunha, J. A.; Hsu, I.-C.; Santos, BS, J. D.;
1217 Lee, J. E.; Sukumar, S.; Larson, P. E. Z.; Vigneron, D. B.; Wilson, D. M.; Sriram, R.;
1218 Kurhanewicz, J. Simultaneous Metabolic and Perfusion Imaging Using Hyperpolarized ^{13}C
1219 MRI Can Evaluate Early and Dose-Dependent Response to Radiation Therapy in a Prostate
1220 Cancer Mouse Model. *Int. J. Radiat. Oncol.* **2020**, *107* (5), 887–896.
1221 <https://doi.org/10.1016/j.ijrobp.2020.04.022>.
- 1222 (85) Golman, K.; Zandt, R. i.; Lerche, M.; Pehrson, R.; Ardenkjaer-Larsen, J. H. Metabolic
1223 Imaging by Hyperpolarized ^{13}C Magnetic Resonance Imaging for *In Vivo* Tumor Diagnosis.
1224 *Cancer Res.* **2006**, *66* (22), 10855–10860. <https://doi.org/10.1158/0008-5472.CAN-06-2564>.
- 1226 (86) Rodrigues, T. B.; Serrao, E. M.; Kennedy, B. W. C.; Hu, D.-E.; Kettunen, M. I.; Brindle, K.
1227 M. Magnetic Resonance Imaging of Tumor Glycolysis Using Hyperpolarized ^{13}C -Labeled
1228 Glucose. *Nat. Med.* **2014**, *20* (1), 93–97. <https://doi.org/10.1038/nm.3416>.
- 1229 (87) Keshari, K. R.; Wilson, D. M.; Chen, A. P.; Bok, R.; Larson, P. E. Z.; Hu, S.; Crieckinge, M.
1230 V.; Macdonald, J. M.; Vigneron, D. B.; Kurhanewicz, J. Hyperpolarized [2- ^{13}C]-Fructose:
1231 A Hemiketal DNP Substrate for *In Vivo* Metabolic Imaging. *J. Am. Chem. Soc.* **2009**, *131*
1232 (48), 17591–17596. <https://doi.org/10.1021/ja9049355>.
- 1233 (88) Utsumi, H.; Hyodo, F. Free Radical Imaging Using *In Vivo* Dynamic Nuclear Polarization-
1234 MRI. In *Methods in Enzymology*; Elsevier, 2015; Vol. 564, pp 553–571.
1235 <https://doi.org/10.1016/bs.mie.2015.08.009>.
- 1236 (89) Saito, K.; Sail, D.; Yamamoto, K.; Matsumoto, S.; Blackman, B.; Kishimoto, S.; Brender, J.
1237 R.; Swenson, R. E.; Mitchell, J. B.; Krishna, M. C. Synthesis and Evaluation of ^{13}C -Labeled
1238 5-5-Dimethyl-1-Pyrroline-N-Oxide Aimed at *in Vivo* Detection of Reactive Oxygen
1239 Species Using Hyperpolarized ^{13}C -MRI. *Free Radic. Biol. Med.* **2019**, *131*, 18–26.
1240 <https://doi.org/10.1016/j.freeradbiomed.2018.11.013>.
- 1241 (90) Franck, J. M.; Kausik, R.; Han, S. Overhauser Dynamic Nuclear Polarization-Enhanced
1242 NMR Relaxometry. *Microporous Mesoporous Mater.* **2013**, *178*, 113–118.
1243 <https://doi.org/10.1016/j.micromeso.2013.04.019>.
- 1244 (91) Neudert, O.; Mattea, C.; Stapf, S. Molecular Dynamics-Based Selectivity for Fast-Field-
1245 Cycling Relaxometry by Overhauser and Solid Effect Dynamic Nuclear Polarization. *J.*
1246 *Magn. Reson.* **2017**, *276*, 113–121. <https://doi.org/10.1016/j.jmr.2017.01.013>.
- 1247 (92) Gizatullin, B.; Mattea, C.; Stapf, S. Overhauser DNP FFC Study of Block Copolymer
1248 Diluted Solution. *Magn. Reson. Imaging* **2019**, *56*, 96–102.
1249 <https://doi.org/10.1016/j.mri.2018.09.005>.
- 1250 (93) Luchinat, C.; Parigi, G. Nuclear Relaxometry Helps Designing Systems for Solution DNP
1251 on Proteins. *Appl. Magn. Reson.* **2008**, *34* (3–4), 379–392. <https://doi.org/10.1007/s00723-008-0116-6>.
- 1253 (94) Parigi, G.; Ravera, E.; Bennati, M.; Luchinat, C. Understanding Overhauser Dynamic
1254 Nuclear Polarisation through NMR Relaxometry. *Mol. Phys.* **2019**, *117* (7–8), 888–897.
1255 <https://doi.org/10.1080/00268976.2018.1527409>.
- 1256 (95) Halse, M. E.; Callaghan, P. T. A Dynamic Nuclear Polarization Strategy for Multi-
1257 Dimensional Earth’s Field NMR Spectroscopy. *J. Magn. Reson.* **2008**, *195* (2), 162–168.
1258 <https://doi.org/10.1016/j.jmr.2008.09.007>.

- 1259 (96) Lee, S.-J.; Shim, J. H.; Kim, K.; Yu, K. K.; Hwang, S. Dynamic Nuclear Polarization in the
1260 Hyperfine-Field-Dominant Region. *J. Magn. Reson.* **2015**, *255*, 114–121.
1261 <https://doi.org/10.1016/j.jmr.2015.04.004>.
- 1262 (97) Yoder, J. L.; Magnelind, P. E.; Espy, M. A.; Janicke, M. T. Exploring the Limits of
1263 Overhauser Dynamic Nuclear Polarization (O-DNP) for Portable Magnetic Resonance
1264 Detection of Low γ Nuclei. *Appl. Magn. Reson.* **2018**, *49* (7), 707–724.
1265 <https://doi.org/10.1007/s00723-018-1014-1>.
- 1266 (98) Zotev, V. S.; Owens, T.; Matlashov, A. N.; Savukov, I. M.; Gomez, J. J.; Espy, M. A.
1267 Microtesla MRI with Dynamic Nuclear Polarization. *J. Magn. Reson.* **2010**, *207* (1), 78–88.
1268 <https://doi.org/10.1016/j.jmr.2010.08.015>.
- 1269 (99) Miloushev, V. Z.; Di Gialleonardo, V.; Salamanca-Cardona, L.; Correa, F.; Granlund, K.
1270 L.; Keshari, K. R. Hyperpolarized ^{13}C Pyruvate Mouse Brain Metabolism with
1271 Absorptive-Mode EPSI at 1 T. *J. Magn. Reson.* **2017**, *275*, 120–126.
1272 <https://doi.org/10.1016/j.jmr.2016.12.009>.
- 1273 (100) van Meerten, S. G. J.; Tayler, M. C. D.; Kentgens, A. P. M.; van Bentum, P. J. M.
1274 Towards Overhauser DNP in Supercritical CO_2 . *J. Magn. Reson.* **2016**, *267*, 30–36.
1275 <https://doi.org/10.1016/j.jmr.2016.04.002>.
- 1276 (101) Sharma, M.; Janssen, G.; Leggett, J.; Kentgens, A. P. M.; van Bentum, P. J. M. Rapid-
1277 Melt Dynamic Nuclear Polarization. *J. Magn. Reson.* **2015**, *258*, 40–48.
1278 <https://doi.org/10.1016/j.jmr.2015.06.007>.
- 1279 (102) Cheng, T.; Capozzi, A.; Takado, Y.; Balzan, R.; Comment, A. Over 35% Liquid-State
1280 ^{13}C Polarization Obtained via Dissolution Dynamic Nuclear Polarization at 7 T and 1 K
1281 Using Ubiquitous Nitroxyl Radicals. *Phys. Chem. Chem. Phys.* **2013**, *15* (48), 20819.
1282 <https://doi.org/10.1039/c3cp53022a>.
- 1283 (103) Cheng, T.; Mishkovsky, M.; Bastiaansen, J. A. M.; Ouari, O.; Hautle, P.; Tordo, P.; van
1284 den Brandt, B.; Comment, A. Automated Transfer and Injection of Hyperpolarized
1285 Molecules with Polarization Measurement Prior to *in Vivo* NMR: Automated Injection
1286 Protocol for *in Vivo* Hyperpolarized NMR. *NMR Biomed.* **2013**, *26* (11), 1582–1588.
1287 <https://doi.org/10.1002/nbm.2993>.
- 1288 (104) Jannin, S.; Comment, A.; Kurdzesau, F.; Konter, J. A.; Hautle, P.; van den Brandt, B.;
1289 van der Klink, J. J. A 140 GHz Prepolarizer for Dissolution Dynamic Nuclear Polarization.
1290 *J. Chem. Phys.* **2008**, *128* (24), 241102. <https://doi.org/10.1063/1.2951994>.
- 1291 (105) Chen, H.-Y.; Hilty, C. Implementation and Characterization of Flow Injection in
1292 Dissolution Dynamic Nuclear Polarization NMR Spectroscopy. *ChemPhysChem* **2015**, *16*
1293 (12), 2646–2652. <https://doi.org/10.1002/cphc.201500292>.
- 1294 (106) Krajewski, M.; Wespi, P.; Busch, J.; Wissmann, L.; Kwiatkowski, G.; Steinhauser, J.;
1295 Batel, M.; Ernst, M.; Kozerke, S. A Multisample Dissolution Dynamic Nuclear Polarization
1296 System for Serial Injections in Small Animals: Multisample Dissolution DNP Polarizer for
1297 Small Animals. *Magn. Reson. Med.* **2017**, *77* (2), 904–910.
1298 <https://doi.org/10.1002/mrm.26147>.
- 1299 (107) Kiswandhi, A.; Niedbalski, P.; Parish, C.; Ferguson, S.; Taylor, D.; McDonald, G.;
1300 Lumata, L. Construction and ^{13}C Hyperpolarization Efficiency of a 180 GHz Dissolution
1301 Dynamic Nuclear Polarization System: A 180 GHz Dissolution DNP System. *Magn. Reson.*
1302 *Chem.* **2017**, *55* (9), 828–836. <https://doi.org/10.1002/mrc.4597>.

- 1303 (108) Balzan, R.; Fernandes, L.; Comment, A.; Pidial, L.; Tavitian, B.; Vasos, P. R. Dissolution
1304 Dynamic Nuclear Polarization Instrumentation for Real-Time Enzymatic Reaction Rate
1305 Measurements by NMR. *J. Vis. Exp.* **2016**, No. 108, 53548. <https://doi.org/10.3791/53548>.
- 1306 (109) Golman, K.; Ardenkjaer-Larsen, J. H.; Petersson, J. S.; Mansson, S.; Leunbach, I.
1307 Molecular Imaging with Endogenous Substances. *Proc. Natl. Acad. Sci.* **2003**, *100* (18),
1308 10435–10439. <https://doi.org/10.1073/pnas.1733836100>.
- 1309 (110) Kiswandhi, A.; Niedbalski, P.; Parish, C.; Ferguson, S.; Taylor, D.; McDonald, G.;
1310 Lumata, L. Construction and ¹³C Hyperpolarization Efficiency of a 180 GHz Dissolution
1311 Dynamic Nuclear Polarization System: A 180 GHz Dissolution DNP System. *Magn. Reson.*
1312 *Chem.* **2017**, *55* (9), 828–836. <https://doi.org/10.1002/mrc.4597>.
- 1313 (111) Thurber, K. R.; Yau, W.-M.; Tycko, R. Low-Temperature Dynamic Nuclear Polarization
1314 at 9.4 T with a 30 mW Microwave Source. *J. Magn. Reson.* **2010**, *204* (2), 303–313.
1315 <https://doi.org/10.1016/j.jmr.2010.03.016>.
- 1316 (112) Bornet, A.; Milani, J.; Vuichoud, B.; Perez Linde, A. J.; Bodenhausen, G.; Jannin, S.
1317 Microwave Frequency Modulation to Enhance Dissolution Dynamic Nuclear Polarization.
1318 *Chem. Phys. Lett.* **2014**, *602*, 63–67. <https://doi.org/10.1016/j.cplett.2014.04.013>.
- 1319 (113) Chen, H.-Y.; Hilty, C. Implementation and Characterization of Flow Injection in
1320 Dissolution Dynamic Nuclear Polarization NMR Spectroscopy. *ChemPhysChem* **2015**, *16*
1321 (12), 2646–2652. <https://doi.org/10.1002/cphc.201500292>.
- 1322 (114) Milani, J.; Vuichoud, B.; Bornet, A.; Miéville, P.; Mottier, R.; Jannin, S.; Bodenhausen,
1323 G. A Magnetic Tunnel to Shelter Hyperpolarized Fluids. *Rev. Sci. Instrum.* **2015**, *86* (2),
1324 024101. <https://doi.org/10.1063/1.4908196>.
- 1325 (115) Kouřil, K.; Kouřilová, H.; Bartram, S.; Levitt, M. H.; Meier, B. Scalable Dissolution-
1326 Dynamic Nuclear Polarization with Rapid Transfer of a Polarized Solid. *Nat. Commun.*
1327 **2019**, *10* (1), 1733. <https://doi.org/10.1038/s41467-019-09726-5>.
- 1328 (116) Pinon, A. C.; Capozzi, A.; Ardenkjær-Larsen, J. H. Hyperpolarized Water through
1329 Dissolution Dynamic Nuclear Polarization with UV-Generated Radicals. *Commun. Chem.*
1330 **2020**, *3* (1), 57. <https://doi.org/10.1038/s42004-020-0301-6>.
- 1331 (117) Ji, X.; Bornet, A.; Vuichoud, B.; Milani, J.; Gajan, D.; Rossini, A. J.; Emsley, L.;
1332 Bodenhausen, G.; Jannin, S. Transportable Hyperpolarized Metabolites. *Nat. Commun.*
1333 **2017**, *8* (1), 13975. <https://doi.org/10.1038/ncomms13975>.
- 1334 (118) Sandra I. Solido. Flow ¹H Dynamic Nuclear Polarization Studies in Normal Liquids and
1335 Supercritical Fluid Carbon Dioxide, Virginia Polytechnic Institute and State University,
1336 2002.
- 1337 (119) Tsai, K. H.; Dorn, H. C. A Model for Establishing the Ultimate Enhancements (A ∞) in
1338 the Low to High Magnetic Field Transfer Dynamic Nuclear Polarization Experiment. *Appl.*
1339 *Magn. Reson.* **1990**, *1* (2), 231–254. <https://doi.org/10.1007/BF03166157>.
- 1340 (120) Dorn, H. C.; Glass, T. E.; Gitti, R.; Tsai, K. H. Transfer Of ¹H And ¹³C Dynamic Nuclear
1341 Polarization from Immobilized Nitroxide Radicals to Flowing Liquids. *Appl. Magn. Reson.*
1342 **1991**, *2* (1), 9–27. <https://doi.org/10.1007/BF03166265>.
- 1343 (121) Gitti, R.; Wild, C.; Tsiao, C.; Zimmer, K.; Glass, T. E.; Dorn, H. C. Solid/Liquid
1344 Intermolecular Transfer of Dynamic Nuclear Polarization. Enhanced Flowing Fluid Proton
1345 NMR Signals via Immobilized Spin Labels. *J. Am. Chem. Soc.* **1988**, *110* (7), 2294–2296.
1346 <https://doi.org/10.1021/ja00215a047>.
- 1347 (122) Kerwood, D. J.; Bolton, P. H. Low-Field NMR. *J. Magn. Reson.* **1969** **1986**, *68* (3), 588–
1348 592. [https://doi.org/10.1016/0022-2364\(86\)90352-5](https://doi.org/10.1016/0022-2364(86)90352-5).

- 1349 (123) Wagner, S.; Dinesen, T. R. J.; Rayner, T.; Bryant, R. G. High-Resolution Magnetic
1350 Relaxation Dispersion Measurements of Solute Spin Probes Using a Dual-Magnet System.
1351 *J. Magn. Reson.* **1999**, *140* (1), 172–178. <https://doi.org/10.1006/jmre.1999.1811>.
- 1352 (124) Redfield, A. G. Shuttling Device for High-Resolution Measurements of Relaxation and
1353 Related Phenomena in Solution at Low Field, Using a Shared Commercial 500 MHz NMR
1354 Instrument. *Magn. Reson. Chem.* **2003**, *41* (10), 753–768. <https://doi.org/10.1002/mrc.1264>.
- 1355 (125) Grosse, S.; Gubaydullin, F.; Scheelken, H.; Vieth, H.-M.; Yurkovskaya, A. V. Field
1356 Cycling by Fast NMR Probe Transfer: Design and Application in Field-Dependent CIDNP
1357 Experiments. *Appl. Magn. Reson.* **1999**, *17* (2–3), 211–225.
1358 <https://doi.org/10.1007/BF03162162>.
- 1359 (126) Grosse, S.; Yurkovskaya, A. V.; Lopez, J.; Vieth, H.-M. Field Dependence of Chemically
1360 Induced Dynamic Nuclear Polarization (CIDNP) in the Photoreaction of *N*-Acetyl
1361 Histidine with 2,2'-Dipyridyl in Aqueous Solution. *J. Phys. Chem. A* **2001**, *105* (26), 6311–
1362 6319. <https://doi.org/10.1021/jp004582i>.
- 1363 (127) Reese, M.; Lennartz, D.; Marquardsen, T.; Höfer, P.; Tavernier, A.; Carl, P.;
1364 Schippmann, T.; Bennati, M.; Carlomagno, T.; Engelke, F.; Griesinger, C. Construction of
1365 a Liquid-State NMR DNP Shuttle Spectrometer: First Experimental Results and Evaluation
1366 of Optimal Performance Characteristics. *Appl. Magn. Reson.* **2008**, *34* (3–4), 301–311.
1367 <https://doi.org/10.1007/s00723-008-0131-7>.
- 1368 (128) Krahn, A.; Lottmann, P.; Marquardsen, T.; Tavernier, A.; Türke, M.-T.; Reese, M.;
1369 Leonov, A.; Bennati, M.; Hofer, P.; Engelke, F.; Griesinger, C. Shuttle DNP Spectrometer
1370 with a Two-Center Magnet. *Phys. Chem. Chem. Phys.* **2010**, *12* (22), 5830.
1371 <https://doi.org/10.1039/c003381b>.
- 1372 (129) Akasaka, K.; Naito, A.; Nakatani, H.; Imanari, M. Construction and Performance of a
1373 Temperature-jump NMR Apparatus. *Rev. Sci. Instrum.* **1990**, *61* (1), 66–68.
1374 <https://doi.org/10.1063/1.1141901>.
- 1375 (130) Joo, C.-G.; Hu, K.-N.; Bryant, J. A.; Griffin, R. G. *In Situ* Temperature Jump High-
1376 Frequency Dynamic Nuclear Polarization Experiments: Enhanced Sensitivity in Liquid-
1377 State NMR Spectroscopy. *J. Am. Chem. Soc.* **2006**, *128* (29), 9428–9432.
1378 <https://doi.org/10.1021/ja0611947>.
- 1379 (131) Joo, C.-G.; Casey, A.; Turner, C. J.; Griffin, R. G. *In Situ* Temperature-Jump Dynamic
1380 Nuclear Polarization: Enhanced Sensitivity in Two-Dimensional ^{13}C – ^{13}C Correlation
1381 Spectroscopy in Solution. *J. Am. Chem. Soc.* **2009**, *131* (1), 12–13.
1382 <https://doi.org/10.1021/ja805521y>.
- 1383 (132) Edward Breeds. Novel Hardware for Temperaturejump DNP. Ph. D. thesis, University of
1384 Nottingham, 2018.
- 1385 (133) Yoon, D.; Soundararajan, M.; Caspers, C.; Braunmueller, F.; Genoud, J.; Alberti, S.;
1386 Ansermet, J.-P. 500-Fold Enhancement of *in Situ* ^{13}C Liquid State NMR Using Gyrotron-
1387 Driven Temperature-Jump DNP. *J. Magn. Reson.* **2016**, *270*, 142–146.
1388 <https://doi.org/10.1016/j.jmr.2016.07.014>.
- 1389 (134) van Meerten, S. G. J.; Janssen, G. E.; Kentgens, A. P. M. Rapid-Melt DNP for
1390 Multidimensional and Heteronuclear High-Field NMR Experiments. *J. Magn. Reson.* **2020**,
1391 *310*, 106656. <https://doi.org/10.1016/j.jmr.2019.106656>.
- 1392 (135) Prandolini, M. J.; Denysenkov, V. P.; Gafurov, M.; Endeward, B.; Prisner, T. F. High-
1393 Field Dynamic Nuclear Polarization in Aqueous Solutions. *J. Am. Chem. Soc.* **2009**, *131*
1394 (17), 6090–6092. <https://doi.org/10.1021/ja901496g>.

- 1395 (136) Denysenkov, V. P.; Prandolini, M. J.; Krahn, A.; Gafurov, M.; Endeward, B.; Prisner, T.
1396 F. High-Field DNP Spectrometer for Liquids. *Appl. Magn. Reson.* **2008**, *34* (3–4), 289–299.
1397 <https://doi.org/10.1007/s00723-008-0127-3>.
- 1398 (137) Höfer, P.; Parigi, G.; Luchinat, C.; Carl, P.; Guthausen, G.; Reese, M.; Carlomagno, T.;
1399 Griesinger, C.; Bennati, M. Field Dependent Dynamic Nuclear Polarization with Radicals
1400 in Aqueous Solution. *J. Am. Chem. Soc.* **2008**, *130* (11), 3254–3255.
1401 <https://doi.org/10.1021/ja0783207>.
- 1402 (138) Liu, G.; Levien, M.; Karschin, N.; Parigi, G.; Luchinat, C.; Bennati, M. One-Thousand-
1403 Fold Enhancement of High Field Liquid Nuclear Magnetic Resonance Signals at Room
1404 Temperature. *Nat. Chem.* **2017**, *9* (7), 676–680. <https://doi.org/10.1038/nchem.2723>.
- 1405 (139) Denysenkov, V.; Prandolini, M. J.; Gafurov, M.; Sezer, D.; Endeward, B.; Prisner, T. F.
1406 Liquid State DNP Using a 260 GHz High Power Gyrotron. *Phys. Chem. Chem. Phys.* **2010**,
1407 *12* (22), 5786. <https://doi.org/10.1039/c003697h>.
- 1408 (140) Dubroca, T.; Smith, A. N.; Pike, K. J.; Froud, S.; Wylde, R.; Trociewitz, B.; McKay, J.;
1409 Mentink-Vigier, F.; van Tol, J.; Wi, S.; Brey, W.; Long, J. R.; Frydman, L.; Hill, S. A
1410 Quasi-Optical and Corrugated Waveguide Microwave Transmission System for
1411 Simultaneous Dynamic Nuclear Polarization NMR on Two Separate 14.1 T Spectrometers.
1412 *J. Magn. Reson.* **2018**, *289*, 35–44. <https://doi.org/10.1016/j.jmr.2018.01.015>.
- 1413 (141) Annino, G.; Villanueva-Garibay, J. A.; van Bentum, P. J. M.; Klaassen, A. A. K.;
1414 Kentgens, A. P. M. A High-Conversion-Factor, Double-Resonance Structure for High-Field
1415 Dynamic Nuclear Polarization. *Appl. Magn. Reson.* **2010**, *37* (1–4), 851–864.
1416 <https://doi.org/10.1007/s00723-009-0091-6>.
- 1417 (142) Jakdetchai, O.; Denysenkov, V.; Becker-Baldus, J.; Dutagaci, B.; Prisner, T. F.; Glaubitz,
1418 C. Dynamic Nuclear Polarization-Enhanced NMR on Aligned Lipid Bilayers at Ambient
1419 Temperature. *J. Am. Chem. Soc.* **2014**, *136* (44), 15533–15536.
1420 <https://doi.org/10.1021/ja509799s>.
- 1421 (143) Fuiiil, Y.; Ishikawa, Y.; Koizumi, Y.; Omija, T.; Ohya, Ik.; Mitsudo, S.; Miura, S.;
1422 Yamamori, H.; Kikuchi, H.; Fukuda, A. Development of Millimeter-Wave Fabry-Perot
1423 Resonator for Simultaneous Electron-Spin and Nuclear-Magnetic Resonance Measurement
1424 at Low Temperatures. In *2018 43rd International Conference on Infrared, Millimeter, and*
1425 *Terahertz Waves (IRMMW-THz)*; IEEE: Nagoya, 2018; pp 1–2.
1426 <https://doi.org/10.1109/IRMMW-THz.2018.8510295>.
- 1427 (144) Fedotov, A.; Kurakin, I.; Fischer, S.; Vogl, T.; Prisner, T. F.; Denysenkov, V. *Increased*
1428 *Flow Rate of Hyperpolarized Aqueous Solution for DNP-Enhanced MRI Achieved by an*
1429 *Open Fabry-Pérot Type Microwave Resonator*; preprint;
1430 Hyperpolarization/Instrumentation, 2020. <https://doi.org/10.5194/mr-2020-20>.
- 1431 (145) Nevzorov, A. A.; Milikisiyants, S.; Marek, A. N.; Smirnov, A. I. Multi-Resonant
1432 Photonic Band-Gap/Saddle Coil DNP Probehead for Static Solid State NMR of Microliter
1433 Volume Samples. *J. Magn. Reson.* **2018**, *297*, 113–123.
1434 <https://doi.org/10.1016/j.jmr.2018.10.010>.
- 1435 (146) Ardenkjær-Larsen, J. H.; Bowen, S.; Petersen, J. R.; Rybalko, O.; Vinding, M. S.;
1436 Ullisch, M.; Nielsen, N. Chr. Cryogen-free Dissolution Dynamic Nuclear Polarization
1437 Polarizer Operating at 3.35 T, 6.70 T, and 10.1 T. *Magn. Reson. Med.* **2019**, *81* (3), 2184–
1438 2194. <https://doi.org/10.1002/mrm.27537>.

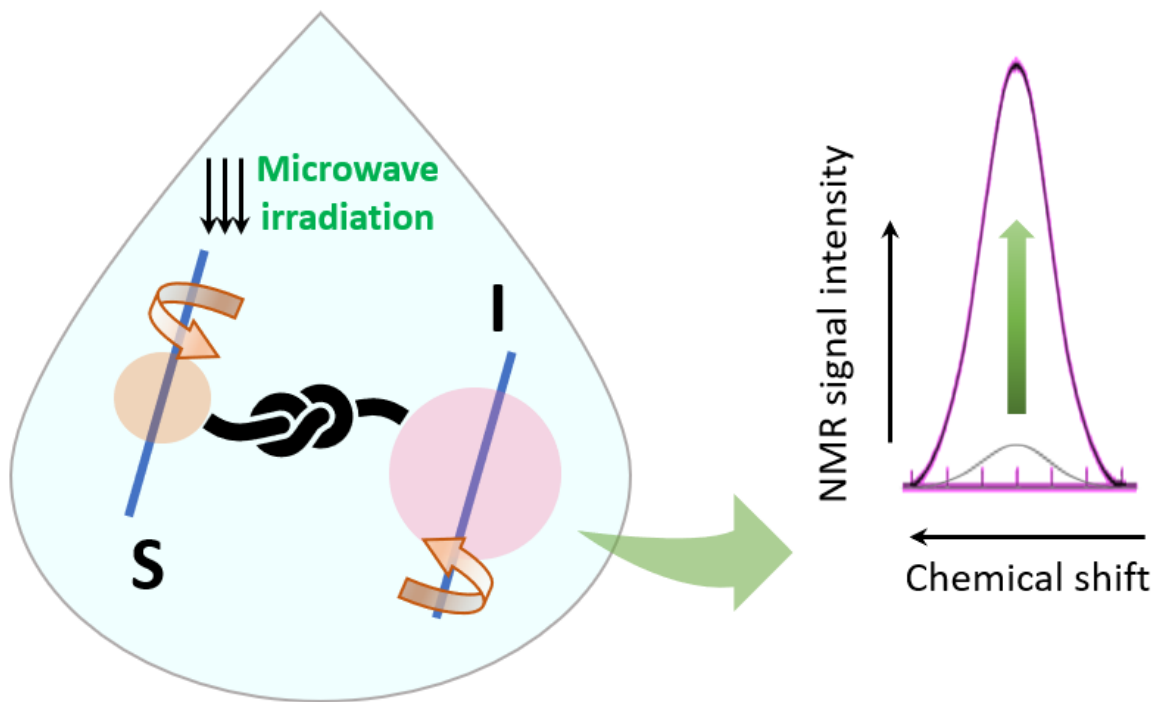
- 1439 (147) Cheng, T.; Gaunt, A. P.; Marco-Rius, I.; Gehrung, M.; Chen, A. P.; Klink, J. J.;
1440 Comment, A. A Multisample 7 T Dynamic Nuclear Polarization Polarizer for Preclinical
1441 Hyperpolarized MR. *NMR Biomed.* **2020**, *33* (5). <https://doi.org/10.1002/nbm.4264>.
- 1442 (148) Bornet, A.; Melzi, R.; Perez Linde, A. J.; Hautle, P.; van den Brandt, B.; Jannin, S.;
1443 Bodenhausen, G. Boosting Dissolution Dynamic Nuclear Polarization by Cross
1444 Polarization. *J. Phys. Chem. Lett.* **2013**, *4* (1), 111–114. <https://doi.org/10.1021/jz301781t>.
- 1445 (149) Song, C.; Hu, K.-N.; Joo, C.-G.; Swager, T. M.; Griffin, R. G. TOTAPOL: A Biradical
1446 Polarizing Agent for Dynamic Nuclear Polarization Experiments in Aqueous Media. *J. Am.*
1447 *Chem. Soc.* **2006**, *128* (35), 11385–11390. <https://doi.org/10.1021/ja061284b>.
- 1448 (150) Sauvée C, Rosay M, Casano G, Aussenac F, Weber RT, Ouari O, Tordo P. Highly
1449 Efficient, Water-Soluble Polarizing Agents for Dynamic Nuclear Polarization at High
1450 Frequency. *Angew Chem Int Ed Engl* **2013**, *52* (41), 10858–10861.
- 1451 (151) Hu, K.-N.; Yu, H.; Swager, T. M.; Griffin, R. G. Dynamic Nuclear Polarization with
1452 Biradicals. *J. Am. Chem. Soc.* **2004**, *126* (35), 10844–10845.
1453 <https://doi.org/10.1021/ja039749a>.
- 1454 (152) Sauvée, C.; Rosay, M.; Casano, G.; Aussenac, F.; Weber, R. T.; Ouari, O.; Tordo, P.
1455 Highly Efficient, Water-Soluble Polarizing Agents for Dynamic Nuclear Polarization at
1456 High Frequency. *Angew. Chem. Int. Ed.* **2013**, *52* (41), 10858–10861.
1457 <https://doi.org/10.1002/anie.201304657>.
- 1458 (153) Lund, A.; Casano, G.; Menzildjian, G.; Kaushik, M.; Stevanato, G.; Yulikov, M.;
1459 Jabbour, R.; Wisser, D.; Renom-Carrasco, M.; Thieuleux, C.; Bernada, F.; Karoui, H.; Siri,
1460 D.; Rosay, M.; Sergeev, I. V.; Gajan, D.; Lelli, M.; Emsley, L.; Ouari, O.; Lesage, A.
1461 TinyPols: A Family of Water-Soluble Binitroxides Tailored for Dynamic Nuclear
1462 Polarization Enhanced NMR Spectroscopy at 18.8 and 21.1 T. *Chem. Sci.* **2020**, *11* (10),
1463 2810–2818. <https://doi.org/10.1039/C9SC05384K>.
- 1464 (154) Ravera, E.; Shimon, D.; Feintuch, A.; Goldfarb, D.; Vega, S.; Flori, A.; Luchinat, C.;
1465 Menichetti, L.; Parigi, G. The Effect of Gd on Trityl-Based Dynamic Nuclear Polarisation
1466 in Solids. *Phys. Chem. Chem. Phys.* **2015**, *17* (40), 26969–26978.
1467 <https://doi.org/10.1039/C5CP04138D>.
- 1468 (155) Lumata, L.; Merritt, M. E.; Malloy, C. R.; Sherry, A. D.; Kovacs, Z. Impact of Gd³⁺ on
1469 DNP of [1- ¹³C]-Pyruvate Doped with Trityl OX063, BDPA, or 4-Oxo-TEMPO. *J. Phys.*
1470 *Chem. A* **2012**, *116* (21), 5129–5138. <https://doi.org/10.1021/jp302399f>.
- 1471 (156) Stevanato, G.; Kubicki, D. J.; Menzildjian, G.; Chauvin, A.-S.; Keller, K.; Yulikov, M.;
1472 Jeschke, G.; Mazzanti, M.; Emsley, L. A Factor Two Improvement in High-Field Dynamic
1473 Nuclear Polarization from Gd(III) Complexes by Design. *J. Am. Chem. Soc.* **2019**, *141* (22),
1474 8746–8751. <https://doi.org/10.1021/jacs.9b03723>.
- 1475 (157) Orlando, T.; Dervişoğlu, R.; Levien, M.; Tkach, I.; Prisner, T. F.; Andreas, L. B.;
1476 Denysenkov, V. P.; Bennati, M. Dynamic Nuclear Polarization of ¹³C Nuclei in the Liquid
1477 State over a 10 Tesla Field Range. *Angew. Chem. Int. Ed.* **2019**, *58* (5), 1402–1406.
1478 <https://doi.org/10.1002/anie.201811892>.
- 1479 (158) Bennati M, O. T. Overhauser DNP in Liquids on ¹³C Nuclei. *eMagRes* **2019**, *8* (1).
- 1480 (159) Levien, M.; Hiller, M.; Tkach, I.; Bennati, M.; Orlando, T. Nitroxide Derivatives for
1481 Dynamic Nuclear Polarization in Liquids: The Role of Rotational Diffusion. *J. Phys. Chem.*
1482 *Lett.* **2020**, *11* (5), 1629–1635. <https://doi.org/10.1021/acs.jpcclett.0c00270>.
- 1483 (160) Lingwood, M. D.; Siaw, T. A.; Sailasuta, N.; Abulseoud, O. A.; Chan, H. R.; Ross, B. D.;
1484 Bhattacharya, P.; Han, S. Hyperpolarized Water as an MR Imaging Contrast Agent:

- 1485 Feasibility of *in Vivo* Imaging in a Rat Model. *Radiology* **2012**, *265* (2), 418–425.
1486 <https://doi.org/10.1148/radiol.12111804>.
- 1487 (161) Vuichoud, B.; Bornet, A.; de Nanteuil, F.; Milani, J.; Canet, E.; Ji, X.; Miéville, P.;
1488 Weber, E.; Kurzbach, D.; Flamm, A.; Konrat, R.; Gossert, A. D.; Jannin, S.; Bodenhausen,
1489 G. Filterable Agents for Hyperpolarization of Water, Metabolites, and Proteins. *Chem. -*
1490 *Eur. J.* **2016**, *22* (41), 14696–14700. <https://doi.org/10.1002/chem.201602506>.
- 1491 (162) McCarney, E. R.; Han, S. Spin-Labeled Gel for the Production of Radical-Free Dynamic
1492 Nuclear Polarization Enhanced Molecules for NMR Spectroscopy and Imaging. *J. Magn.*
1493 *Reson.* **2008**, *190* (2), 307–315. <https://doi.org/10.1016/j.jmr.2007.11.013>.
- 1494 (163) Cheng, T.; Mishkovsky, M.; Junk, M. J. N.; Münnemann, K.; Comment, A. Producing
1495 Radical-Free Hyperpolarized Perfusion Agents for *In Vivo* Magnetic Resonance Using
1496 Spin-Labeled Thermoresponsive Hydrogel. *Macromol. Rapid Commun.* **2016**, *37* (13),
1497 1074–1078. <https://doi.org/10.1002/marc.201600133>.
- 1498 (164) Capozzi, A.; Cheng, T.; Boero, G.; Roussel, C.; Comment, A. Thermal Annihilation of
1499 Photo-Induced Radicals Following Dynamic Nuclear Polarization to Produce Transportable
1500 Frozen Hyperpolarized ¹³C-Substrates. *Nat. Commun.* **2017**, *8* (1), 15757.
1501 <https://doi.org/10.1038/ncomms15757>.
- 1502 (165) Capozzi, A.; Patel, S.; Gunnarsson, C. P.; Marco-Rius, I.; Comment, A.; Karlsson, M.;
1503 Lerche, M. H.; Ouari, O.; Ardenkjaer-Larsen, J. H. Efficient Hyperpolarization of U- ¹³C-
1504 Glucose Using Narrow-Line UV-Generated Labile Free Radicals. *Angew. Chem. Int. Ed.*
1505 **2019**, *58* (5), 1334–1339. <https://doi.org/10.1002/anie.201810522>.
- 1506 (166) Henstra, A.; Lin, T.-S.; Schmidt, J.; Wenckebach, W. Th. High Dynamic Nuclear
1507 Polarization at Room Temperature. *Chem. Phys. Lett.* **1990**, *165* (1), 6–10.
1508 [https://doi.org/10.1016/0009-2614\(90\)87002-9](https://doi.org/10.1016/0009-2614(90)87002-9).
- 1509 (167) Kagawa, A.; Negoro, M.; Ohba, R.; Ichijo, N.; Takamine, K.; Nakamura, Y.; Murata, T.;
1510 Morita, Y.; Kitagawa, M. Dynamic Nuclear Polarization Using Photoexcited Triplet
1511 Electron Spins in Eutectic Mixtures. *J. Phys. Chem. A* **2018**, *122* (50), 9670–9675.
1512 <https://doi.org/10.1021/acs.jpca.8b09934>.
- 1513 (168) Negoro, M.; Kagawa, A.; Tateishi, K.; Tanaka, Y.; Yuasa, T.; Takahashi, K.; Kitagawa,
1514 M. Dissolution Dynamic Nuclear Polarization at Room Temperature Using Photoexcited
1515 Triplet Electrons. *J. Phys. Chem. A* **2018**, *122* (17), 4294–4297.
1516 <https://doi.org/10.1021/acs.jpca.8b01415>.
- 1517 (169) Kagawa, A.; Miyanishi, K.; Ichijo, N.; Negoro, M.; Nakamura, Y.; Enozawa, H.; Murata,
1518 T.; Morita, Y.; Kitagawa, M. High-Field NMR with Dissolution Triplet-DNP. *J. Magn.*
1519 *Reson.* **2019**, *309*, 106623. <https://doi.org/10.1016/j.jmr.2019.106623>.
- 1520 (170) Kouno, H.; Kawashima, Y.; Tateishi, K.; Uesaka, T.; Kimizuka, N.; Yanai, N.
1521 Nonpentacene Polarizing Agents with Improved Air Stability for Triplet Dynamic Nuclear
1522 Polarization at Room Temperature. *J. Phys. Chem. Lett.* **2019**, *10* (9), 2208–2213.
1523 <https://doi.org/10.1021/acs.jpcllett.9b00480>.
- 1524 (171) Kouno, H.; Orihashi, K.; Nishimura, K.; Kawashima, Y.; Tateishi, K.; Uesaka, T.;
1525 Kimizuka, N.; Yanai, N. Triplet Dynamic Nuclear Polarization of Crystalline Ice Using
1526 Water-Soluble Polarizing Agents. *Chem. Commun.* **2020**, *56* (26), 3717–3720.
1527 <https://doi.org/10.1039/D0CC00836B>.
- 1528 (172) Liu, G.; Liou, S.-H.; Enkin, N.; Tkach, I.; Bennati, M. Photo-Induced Radical
1529 Polarization and Liquid-State Dynamic Nuclear Polarization Using Fullerene Nitroxide

1530 Derivatives. *Phys. Chem. Chem. Phys.* **2017**, *19* (47), 31823–31829.
1531 <https://doi.org/10.1039/C7CP06073D>.
1532 (173) Schroeder, F. C.; Gronquist, M. Extending the Scope of NMR Spectroscopy with
1533 Microcoil Probes. *Angew. Chem. Int. Ed.* **2006**, *45* (43), 7122–7131.
1534 <https://doi.org/10.1002/anie.200601789>.
1535 (174) Fratila, R. M.; Velders, A. H. Small-Volume Nuclear Magnetic Resonance Spectroscopy.
1536 *Annu. Rev. Anal. Chem.* **2011**, *4* (1), 227–249. [https://doi.org/10.1146/annurev-anchem-](https://doi.org/10.1146/annurev-anchem-061010-114024)
1537 [061010-114024](https://doi.org/10.1146/annurev-anchem-061010-114024).
1538 (175) Lee, J. H.; Okuno, Y.; Cavagnero, S. Sensitivity Enhancement in Solution NMR:
1539 Emerging Ideas and New Frontiers. *J. Magn. Reson.* **2014**, *241*, 18–31.
1540 <https://doi.org/10.1016/j.jmr.2014.01.005>.
1541 (176) Luchinat, E.; Banci, L. In-Cell NMR: A Topical Review. *IUCrJ* **2017**, *4* (2), 108–118.
1542 <https://doi.org/10.1107/S2052252516020625>.
1543 (177) Mousoulis, C.; Xu, X.; Reiter, D. A.; Neu, C. P. Single Cell Spectroscopy: Noninvasive
1544 Measures of Small-Scale Structure and Function. *Methods* **2013**, *64* (2), 119–128.
1545 <https://doi.org/10.1016/j.ymeth.2013.07.025>.
1546 (178) Gökay, O.; Albert, K. From Single to Multiple Microcoil Flow Probe NMR and Related
1547 Capillary Techniques: A Review. *Anal. Bioanal. Chem.* **2012**, *402* (2), 647–669.
1548 <https://doi.org/10.1007/s00216-011-5419-z>.
1549 (179) Guo, J.; Jiang, D.; Feng, S.; Ren, C.; Guo, J. M-NMR at the Point of Care Testing.
1550 *ELECTROPHORESIS* **2020**, *41* (5–6), 319–327. <https://doi.org/10.1002/elps.201900329>.
1551 (180) Sahin Solmaz, N.; Grisi, M.; Matheoud, A. V.; Gualco, G.; Boero, G. Single-Chip
1552 Dynamic Nuclear Polarization Microsystem. *Anal. Chem.* **2020**, *92* (14), 9782–9789.
1553 <https://doi.org/10.1021/acs.analchem.0c01221>.
1554 (181) Keller, T. J.; Laut, A. J.; Sirigiri, J.; Maly, T. High-Resolution Overhauser Dynamic
1555 Nuclear Polarization Enhanced Proton NMR Spectroscopy at Low Magnetic Fields. *J.*
1556 *Magn. Reson.* **2020**, *313*, 106719. <https://doi.org/10.1016/j.jmr.2020.106719>.
1557

1558

1559 TOC Graphic:



1560

1561

1562



Veronika Szalai joined the National Institute of Standards & Technology (NIST) in 2010 and is currently a Project Leader in the Biophysical and Biomedical Measurement Group. She received an A.B. in Chemistry from Bryn Mawr College and a Ph.D. in Inorganic Chemistry from Yale University. After completing post-doctoral work at the University of North Carolina at Chapel Hill, Veronika advanced to the rank of associate professor (with tenure) in the Department of Chemistry & Biochemistry at the University of Maryland Baltimore County. Her laboratory at NIST focuses on advanced electron paramagnetic resonance (EPR) spectroscopy and instrumentation development for measurements of biological and nanomaterial systems and, previously, on tools for *in operando* reactivity measurements of nanomaterials.

1577



Nandita Abhyankar is a Visiting Fellow working jointly at the Institute for Research in Applied Physics and Electronics (IREAP) at UMD, College Park and the Physical Measurement Laboratory (PML) at NIST. Here she works on designing, fabricating, and implementing microresonators for electron paramagnetic resonance (EPR) spectroscopy. She obtained an M.S. in Chemistry from Pune University in India and her Ph.D. in Physical Chemistry from Florida State University, where she worked on methods for synthesizing metal-organic frameworks (MOFs) and studying their electric and magnetic properties.

1590